

# Enhanced Uplink Data Detection for Massive MIMO with 1-Bit ADCs: Analysis and Joint Detection

Amin Radbord, Italo Atzeni, and Antti Tölli

**Abstract**—We present a new analytical framework on the uplink data detection for massive multiple-input multiple-output systems with 1-bit analog-to-digital converters (ADCs). We first characterize the expected values of the soft-estimated symbols (after the linear receiver and prior to the data detection), which are affected by the 1-bit quantization during both the channel estimation and the uplink data transmission. In our analysis, we consider conventional receivers such as maximum ratio combining (MRC), zero forcing, and minimum mean squared error (MMSE), with multiple user equipments (UEs) and correlated Rayleigh fading. Additionally, we design a linear minimum mean dispersion (LMMD) receiver tailored for the data detection with 1-bit ADCs, which exploits the expected values of the soft-estimated symbols previously derived. Then, we propose a joint data detection (JD) strategy that exploits the interdependence among the soft-estimated symbols of the interfering UEs, along with its low-complexity variant. These strategies are compared with the robust maximum likelihood data detection with 1-bit ADCs. Numerical results examining the symbol error rate show that MMSE exhibits a considerable performance gain over MRC, whereas the proposed LMMD receiver significantly outperforms all the conventional receivers. Lastly, the proposed JD and its low-complexity variant provide a significant boost in comparison with the single-UE data detection.

**Index Terms**—1-bit ADCs, joint data detection, massive MIMO.

## I. INTRODUCTION

To leverage the wide bandwidths in the (sub-)THz spectrum, massive multiple-input multiple-output (MIMO) arrays are required at the transmitter and/or receiver to overcome the strong pathloss and penetration loss [3], [4]. In this respect, fully digital massive MIMO architectures with low-resolution analog-to-digital/digital-to-analog converters (ADCs/DACs) can provide highly flexible beamforming and large-scale spatial multiplexing with modest power consumption and complexity without excessively compromising the spectral efficiency [5]–[7]. Remarkably, fully-digital massive MIMO systems with few-bit or even 1-bit ADCs/DACs can outperform hybrid analog-digital ones in terms of both spectral and energy efficiency [8].

The data detection in 1-bit quantized massive MIMO systems has been the subject of many recent studies. An asymptotic closed-form approximation of the symbol error rate (SER) with the quantized zero-forcing (ZF) precoder is derived in [9] for downlink massive MIMO with 1-bit DACs. However, this SER approximation is only applicable when the channel is

perfectly known at each user equipments (UE). In the context of uplink data detection, a two-stage near maximum likelihood (ML) data detection method is proposed in [10], which reduces the number of candidate transmit vectors by leveraging the output of the one-stage near ML detector. It also utilizes the ML detector structure to enhance the data detection performance of the initial one-stage near ML detector. A low-complexity message passing de-quantization detector (MPDQD) is developed in [11], which exploits both the structured sparsity and the prior probability distribution of the transmitted signal. A sphere decoding method for the uplink massive MIMO with 1-bit ADCs is proposed in [12], where the weighted Hamming distance is exploited to construct a list of codewords for sphere decoding to account for the discrete nature of the received signal. Assuming perfect channel state information (CSI) and a large number of UEs, an MPDQ algorithm via Gaussian belief propagation based on the Bussgang theorem is presented in [13] for the uplink data detection in millimeter-wave systems with low-resolution ADCs. A robust ML (RML) method with nearest-neighbor (NN) search is proposed in [14] for multi-UE systems with imperfect CSI. In addition, recent works have shown that machine learning approaches can be utilized to provide efficient and robust channel estimation and data detection in massive MIMO systems with 1-bit ADCs [14]–[16]. For instance, a two-stage data detection algorithm based on a support vector machine is devised in [16]. The performance of this data detection method is very close to that of ML when perfect CSI is available. Although all of these works focus on designing low-complexity and accurate data detection methods to improve the system performance, they only use the original transmit constellation as a reference.

The expected values of the soft-estimated symbols (after the linear receiver and prior to the data detection) were characterized in [17], [18] for a massive single-input multiple-output (SIMO) system with 1-bit ADCs. These expected values effectively capture the distortion in the transmit constellation due to the 1-bit quantization during both the channel estimation and the uplink data transmission, which directly depends on the signal-to-noise ratio (SNR). In this respect, it is demonstrated in [17] that the distortion at high SNR is such that the soft-estimated symbols resulting from the data symbols with the same phase become indistinguishable. Hence, the amplitude information cannot be recovered at very high SNR. Simple single-UE data detection strategies based on the expected values of the soft-estimated symbols are proposed in [19] for independent and identically distributed (i.i.d.) Rayleigh fading

The authors are with the Centre for Wireless Communications, University of Oulu, Finland (e-mail: {amin.radbord, italo.atzeni, antti.tolli}@oulu.fi). Part of this work was presented at IEEE ICASSP 2023 [1] and ASILOMAR 2023 [2].

channels.

### A. Contribution

In this paper, we extend the previous work [17], which characterized the expected values of the soft-estimated symbols for a simplified system model with a single UE and i.i.d. Rayleigh fading. However, uncorrelated channel models cannot account for the sparse scattering at high frequencies. Here, we consider a more general and realistic multi-UE setting with correlated Rayleigh fading. Furthermore, while the analysis in [17] is only limited to maximum ratio combining (MRC), we extend it to the ZF and minimum mean squared error (MMSE) receivers. Additionally, we design a *linear minimum mean dispersion* (LMMD) receiver tailored for the data detection with 1-bit ADCs, which exploits the expected values of the soft-estimated symbols previously derived. Furthermore, we propose a joint data detection (JD) strategy that exploits the interdependence among the soft-estimated symbols of the interfering UEs, along with its low-complexity variant.

The contributions of this paper are summarized as follows:

- We first characterize the expected values of the soft-estimated symbols for a multi-UE setting when the MRC receiver is adopted at the base station (BS). The characterization of these expected values is of particular interest since they effectively capture the distortion in the transmit constellation due to the 1-bit quantization during both the channel estimation and the uplink data transmission, which directly depends on the SNR. Our results show that the expected value of the soft-estimated symbol of a specific UE depends on the SNR, the number of UEs, the number of BS antennas, the pilot sequence, and the data symbols transmitted by all the UEs. These results can be exploited to take advantage of the specific data symbols transmitted by the interfering UEs, thereby improving the data detection performance.
- Then, we broaden the theoretical analysis of the expected values of the soft-estimated symbols as well as the numerical evaluation when the ZF and MMSE receivers are adopted at the BS. Interestingly, these expected values can be asymptotically obtained with simple scaling of their MRC counterparts, for which we derived the closed-form expression earlier. We derive an asymptotic closed-form expression of this scaling.
- For the receiver design tailored for the data detection with 1-bit ADCs, we take into account the impact of the expected values of the soft-estimated symbols. We propose LMMD receiver that minimizes the mean dispersion of the soft-estimated symbols around the expected values obtained with the conventional receivers, i.e., MRC, ZF, and MMSE.
- For the data detection with 1-bit ADCs, we propose new data detection strategies based on the minimum distance criterion with respect to the expected values of the soft-estimated symbols. In this respect, first, we introduce some single-UE data detection strategies, such as exhaustive, heuristic, and genie-aided data detection. These single-UE strategies are just intermediate steps to see how we can take advantage of the interdependence

among the soft-estimated symbols of the interfering UEs in order to improve SER. Then, we propose an enhanced multi-UE data detection strategy as JD that considers parallel data detection over all the UEs and exploits the interdependence among their soft-estimated symbols. Lastly, we present a low-complexity variant of JD obtained by reducing the size of the search space.

- Numerical results show that the proposed LMMD receiver provides substantial performance gain in terms of SER compared with the conventional receivers, i.e., MRC and MMSE. Furthermore, among the conventional receivers, MMSE shows substantial performance gain with respect to MRC, thanks to the reduced dispersion of the soft-estimated symbols around their expected values. In addition, the proposed JD and its low-complexity variant greatly outperform the single-UE data detection since the latter does not account for the interdependence among the soft-estimated symbols of the interfering UEs.

Part of this work is included in our conference papers [1], [2]. Specifically, [1] derives the closed-form expression of the expected values of the soft-estimated symbols obtained with MRC in a multi-UE setting and proposes single-UE data detection strategies. On the other hand, [2] provides a numerical evaluation of the expected values of the soft-estimated symbols obtained with the ZF and MMSE receivers and introduces JD. In this paper, we analytically characterize the expected values of the soft-estimated symbols obtained with the ZF and MMSE receivers and propose a novel receiver design tailored for the data detection with 1-bit ADCs, which is based on the expected values of the soft-estimated symbols previously derived. Moreover, we present comprehensive numerical results considering a variety of system parameters.

*Outline.* The rest of the paper is structured as follows. Section II introduces the system model. Section III characterizes the expected values of the soft-estimated symbols obtained with the conventional receivers. Section IV exploits this result to propose a new receiver design tailored for the data detection with 1-bit ADCs. Section V presents novel data detection strategies. Section VI provides the numerical results and discussion. Lastly, Section VII draws some concluding remarks.

*Notation.*  $(\cdot)^T$ ,  $(\cdot)^H$ , and  $(\cdot)^*$  represent transpose, Hermitian transpose, and conjugate, respectively.  $\text{Re}[\cdot]$  and  $\text{Im}[\cdot]$  denote the real part and imaginary parts, respectively, whereas  $j$  is the imaginary unit.  $\mathbb{E}[\cdot]$  is the expectation operator.  $\mathbf{I}_N$  and  $\mathbf{0}_N$  denote the  $N$ -dimensional identity matrix and all-zero vector, respectively.  $[\cdot]_{m,n}$  specifies the  $(m, n)$ th element of the matrix argument.  $\{\cdot\}$  is used to denote sets.  $\text{vec}[\cdot]$  is the vectorization operator.  $\otimes$  denotes the Kronecker product.  $\text{sgn}(\cdot)$  is the sign function.  $\text{diag}(\cdot)$  produces a diagonal matrix with the elements of the vector argument or the diagonal elements of the square matrix argument on its diagonal.  $\text{blkdiag}(\cdot)$  produces a block-diagonal matrix.  $\mathcal{CN}(\mathbf{0}_N, \Sigma)$  and  $\mathcal{N}(\mathbf{0}_N, \Sigma)$  are, respectively, the  $N$ -variate complex and real normal distributions with zero mean and covariance matrix  $\Sigma$ .  $\Phi(x) \triangleq \frac{2}{\sqrt{\pi}} \int_0^x e^{-t^2} dt$  represents the error function.

## II. SYSTEM MODEL

Consider a single-cell massive MIMO system where a BS equipped with  $M$  antennas serves  $K$  single-antenna UEs in the uplink. Let  $\mathbf{H} \triangleq [\mathbf{h}_1, \dots, \mathbf{h}_K] \in \mathbb{C}^{M \times K}$  denote the uplink channel matrix, where  $\mathbf{h}_k$  represents the channel vector of UE  $k$ . Considering a general correlated Rayleigh fading channel model, we have  $\mathbf{h}_k \sim \mathcal{CN}(\mathbf{0}_M, \mathbf{C}_{\mathbf{h}_k})$ ,  $\forall k = 1, \dots, K$ , where  $\mathbf{C}_{\mathbf{h}_k} \in \mathbb{C}^{M \times M}$  is the channel covariance matrix of UE  $k$ . Furthermore, we define  $\mathbf{h} \triangleq \text{vec}(\mathbf{H}) \in \mathbb{C}^{MK}$  and, accordingly, we have  $\mathbf{h} \sim \mathcal{CN}(\mathbf{0}_{MK}, \mathbf{C}_{\mathbf{h}})$ , with  $\mathbf{C}_{\mathbf{h}} \triangleq \text{blkdiag}(\mathbf{C}_{\mathbf{h}_1}, \dots, \mathbf{C}_{\mathbf{h}_K}) \in \mathbb{C}^{MK \times MK}$ . For simplicity and without loss of generality, we assume that all the UEs are subject to the same SNR  $\rho$  during both the channel estimation and the uplink data transmission (as done, e.g., in [5], [6], [17]). Each BS antenna is connected to two 1-bit ADCs, one for the in-phase and one for the quadrature component of the received signal. In this context, we introduce the 1-bit quantization function  $Q(\cdot) : \mathbb{C}^{A \times B} \rightarrow \mathcal{Q}$ , with  $\mathcal{Q} \triangleq \sqrt{\frac{\rho K + 1}{2}} \{\pm 1 \pm j\}^{A \times B}$  and

$$Q(\mathbf{X}) \triangleq \sqrt{\frac{\rho K + 1}{2}} \left( \text{sgn}(\text{Re}[\mathbf{X}]) + j \text{sgn}(\text{Im}[\mathbf{X}]) \right). \quad (1)$$

### A. Channel Estimation

As in [5], we utilize the Busgang linear MMSE (BLMMSE) estimator to estimate the channels. Let  $\mathbf{P} \triangleq [\mathbf{p}_1, \dots, \mathbf{p}_K] \in \mathbb{C}^{\tau \times K}$  denote the pilot matrix, where  $\tau$  is the pilot length,  $\mathbf{p}_k \in \mathbb{C}^\tau$  represents the pilot vector of UE  $k$ , and  $P_{u,k}$  is the  $(u, k)$ th element of  $\mathbf{P}$ . We assume  $\tau \geq K$  and orthogonal pilots among the UEs. During the channel estimation, all the UEs simultaneously transmit their pilots, and the signal received at the input of the ADCs at the BS is given by

$$\mathbf{Y}_p \triangleq \sqrt{\rho} \mathbf{H} \mathbf{P} + \mathbf{Z}_p \in \mathbb{C}^{M \times \tau} \quad (2)$$

where  $\mathbf{Z}_p \in \mathbb{C}^{M \times \tau}$  is a matrix of AWGN with i.i.d.  $\mathcal{CN}(0, 1)$  elements. At this stage, we vectorize (2) as

$$\mathbf{y}_p \triangleq \text{vec}(\mathbf{Y}_p) = \sqrt{\rho} \bar{\mathbf{P}} \mathbf{h} + \mathbf{z}_p \in \mathbb{C}^{M\tau} \quad (3)$$

with  $\bar{\mathbf{P}} \triangleq \mathbf{P} \otimes \mathbf{I}_M \in \mathbb{C}^{M\tau \times MK}$  and  $\mathbf{z}_p \triangleq \text{vec}(\mathbf{Z}_p) \in \mathbb{C}^{M\tau}$ . The BS observes the quantized signal

$$\mathbf{r}_p \triangleq Q(\mathbf{y}_p) \in \mathbb{C}^{M\tau} \quad (4)$$

and obtains an estimate of  $\mathbf{h}$  via the BLMMSE estimator as [5]

$$\hat{\mathbf{h}} \triangleq \sqrt{\rho} \mathbf{C}_{\mathbf{h}} \bar{\mathbf{P}}^T \mathbf{A}_p \mathbf{C}_{\mathbf{r}_p}^{-1} \mathbf{r}_p \in \mathbb{C}^{MK} \quad (5)$$

with  $\mathbf{C}_{\mathbf{r}_p} \triangleq \mathbb{E}[\mathbf{r}_p \mathbf{r}_p^H] \in \mathbb{C}^{M\tau \times M\tau}$  and where

$$\mathbf{A}_p \triangleq \sqrt{\frac{2}{\pi}} (\rho K + 1) \text{diag}(\mathbf{C}_{\mathbf{y}_p})^{-\frac{1}{2}} \in \mathbb{C}^{M\tau \times M\tau} \quad (6)$$

is the Busgang gain matrix, with  $\mathbf{C}_{\mathbf{y}_p} \triangleq \mathbb{E}[\mathbf{y}_p \mathbf{y}_p^H] = \rho \bar{\mathbf{P}} \mathbf{C}_{\mathbf{h}} \bar{\mathbf{P}}^T + \mathbf{I}_{M\tau} \in \mathbb{C}^{M\tau \times M\tau}$ . Finally, the estimate of  $\mathbf{H}$  is expressed as  $\hat{\mathbf{H}} \triangleq [\hat{\mathbf{h}}_1, \dots, \hat{\mathbf{h}}_K] \in \mathbb{C}^{M \times K}$ , with

$$\hat{\mathbf{h}}_k \triangleq \sqrt{\rho} \mathbf{C}_{\mathbf{h}_k} \bar{\mathbf{P}}_k^T \mathbf{A}_p \mathbf{C}_{\mathbf{r}_p}^{-1} \mathbf{r}_p \in \mathbb{C}^M \quad (7)$$

and  $\bar{\mathbf{P}}_k \triangleq \mathbf{p}_k \otimes \mathbf{I}_M \in \mathbb{C}^{M\tau \times M}$ .

### B. Uplink Data Transmission

Let  $\mathbf{x} \triangleq [x_1, \dots, x_K]^T \in \mathbb{C}^K$  denote the data symbol vector comprising the data symbols transmitted by the

UEs. Moreover, let  $\mathbf{x} \in \mathcal{S}^K$ , where  $\mathcal{S} \triangleq \{s_1, \dots, s_L\}$  represents the transmit constellation with  $L$  data symbols. We use  $l_k \in \{1, \dots, L\}$  to denote the index of the data symbol from  $\mathcal{S}$  transmitted by UE  $k$ . In this paper, we assume that  $\mathcal{S}$  corresponds to the 16-QAM constellation, i.e.,  $\mathcal{S} = \frac{1}{\sqrt{10}} \{\pm 1 \pm j, \pm 1 \pm j3, \pm 3 \pm j, \pm 3 \pm j3\}$ , which is normalized such that  $\frac{1}{L} \sum_{l=1}^L |s_l|^2 = 1$ . Nonetheless, our analysis and data detection algorithms are general and can be applied to any transmit constellation. During the uplink data transmission, all the UEs simultaneously transmit their data symbols, and the signal received at the input of the ADCs at the BS is given by

$$\mathbf{y} \triangleq \sqrt{\rho} \mathbf{H} \mathbf{x} + \mathbf{z} \in \mathbb{C}^M \quad (8)$$

where  $\mathbf{z} \sim \mathcal{CN}(\mathbf{0}_M, \mathbf{I}_M)$  is a vector of AWGN. The BS observes the quantized signal

$$\mathbf{r} \triangleq Q(\mathbf{y}) \in \mathbb{C}^M \quad (9)$$

where we note that the scaling factor  $\sqrt{\frac{\rho K + 1}{2}}$  in (1) is set such that the variance of  $\mathbf{r}$  coincides with that of  $\mathbf{y}$  (see, e.g., [6], [17]). Then, the BS obtains a soft estimate of  $\mathbf{x}$  via linear combining as

$$\hat{\mathbf{x}} \triangleq [\hat{x}_1, \dots, \hat{x}_K]^T = \mathbf{V}^H \mathbf{r} \in \mathbb{C}^K \quad (10)$$

where  $\mathbf{V} \in \mathbb{C}^{M \times K}$  is the receiver matrix based on imperfect CSI, which is carried out as described in Section II-A. In this paper, we consider the conventional receivers obtained by plugging the channel estimated with 1-bit ADCs into the well-known MRC, ZF, and MMSE structures, i.e.,

$$\mathbf{V}^{(\text{MRC})} = \hat{\mathbf{H}}, \quad (11)$$

$$\mathbf{V}^{(\text{ZF})} = \hat{\mathbf{H}} (\hat{\mathbf{H}}^H \hat{\mathbf{H}})^{-1}, \quad (12)$$

$$\mathbf{V}^{(\text{MMSE})} = (\rho \hat{\mathbf{H}} \hat{\mathbf{H}}^H + \mathbf{I}_M)^{-1} \hat{\mathbf{H}}. \quad (13)$$

These conventional receivers, which are inherited from infinite-resolution systems, ignore the non-linear effects of the 1-bit ADCs. Therefore, in Section IV, we propose a novel receiver design tailored for the data detection with 1-bit ADCs.

## III. EXPECTATION OF THE SOFT-ESTIMATED SYMBOLS

The prior work [17] focused on a single-UE setting with i.i.d. Rayleigh fading and analytically characterized the statistical properties (i.e., expected value and variance) of the soft-estimated symbols, which depend on the data symbol and pilot of the UE. In this paper, we consider a more general and realistic multi-UE setting with correlated Rayleigh fading. In this section, we derive a closed-form expression of the expected values of the soft-estimated symbols obtained with the MRC receiver and then connect it through approximations to the cases of ZF and MMSE receivers. We show that these expected values depend on the data symbol vector  $\mathbf{x}$  and pilot matrix  $\mathbf{P}$ .

### A. Expected Values of the Soft-Estimated Symbols with MRC

Here, we assume that the MRC receiver is adopted at the BS, where the receiver matrix is given in (11). Hence, the soft-estimated symbol of UE  $k$  can be expressed as  $\hat{x}_k^{(\text{MRC})} = \hat{\mathbf{h}}_k^H \mathbf{r}$ , with  $\hat{\mathbf{h}}_k$  and  $\mathbf{r}$  given in (7) and (9), respectively. Let us

$$[\mathbf{C}_{\mathbf{r}_p}]_{(u-1)M+m,(v-1)M+n} = \begin{cases} \rho K + 1 & \text{if } m = n \text{ and } u = v, \\ (\rho K + 1) \left( \Omega(\text{Re}[\zeta_{m,n,u,v}]) - j \Omega(\text{Im}[\zeta_{m,n,u,v}]) \right) & \text{otherwise} \end{cases} \quad (19)$$

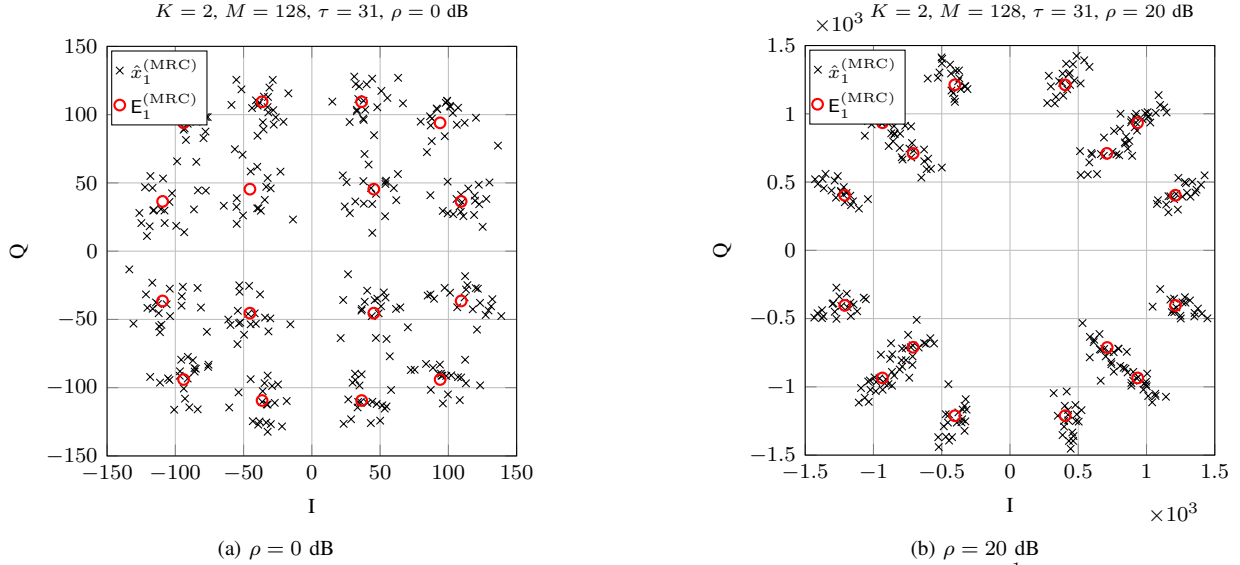


Fig. 1. Soft-estimated symbols (black markers) and their expected values (red markers) of UE 1 when  $x_2 = \frac{1}{\sqrt{10}}(-1 + j)$ ; the MRC receiver is adopted at the BS.

define  $\mathbf{C}_{\mathbf{r}_p} \triangleq \mathbb{E}[\mathbf{r}_p \mathbf{r}_p^H] \in \mathbb{C}^{M \times M\tau}$ , which represents the cross-covariance matrix between the quantized signals received during the uplink data transmission and the channel estimation. Moreover, we introduce the function  $\Omega(x) \triangleq \frac{2}{\pi} \arcsin(x)$  and the following preliminary definitions:

$$\alpha_m \triangleq \left[ \rho \sum_{k=1}^K \mathbf{C}_{\mathbf{h}_k} + \mathbf{I}_M \right]_{m,m}, \quad (14)$$

$$\beta_m \triangleq \left[ \rho \sum_{k=1}^K \mathbf{C}_{\mathbf{h}_k} |x_k|^2 + \mathbf{I}_M \right]_{m,m}, \quad (15)$$

$$\zeta_{m,n,u,v} \triangleq \frac{\rho}{\sqrt{\alpha_m \alpha_n}} \left[ \sum_{k=1}^K \mathbf{C}_{\mathbf{h}_k}^T P_{u,k} P_{v,k}^* \right]_{m,n}, \quad (16)$$

$$\eta_{m,n,u} \triangleq \frac{\rho}{\sqrt{\alpha_n \beta_m}} \left[ \sum_{k=1}^K \mathbf{C}_{\mathbf{h}_k} x_k P_{u,k} \right]_{m,n}. \quad (17)$$

The following theorem provides a closed-form expression of the expected value of the soft-estimated symbol of UE  $k$  obtained with the MRC receiver for a given data symbol vector  $\mathbf{x}$ . This is denoted by  $\mathbf{E}_k^{(\text{MRC})}(\mathbf{x}, \mathbf{P}) \triangleq \mathbb{E}_{\mathbf{H}, \mathbf{z}, \mathbf{z}_p}[\hat{x}_k^{(\text{MRC})}]$ .

**Theorem 1.** Assuming that the MRC receiver is adopted at the BS, for a given data symbol vector  $\mathbf{x}$  and pilot matrix  $\mathbf{P}$ , the expected value of the soft-estimated symbol of UE  $k$  is given by

$$\mathbf{E}_k^{(\text{MRC})}(\mathbf{x}, \mathbf{P}) = \sqrt{\rho} \text{tr}(\mathbf{C}_{\mathbf{r}_p}^{-1} \mathbf{A}_p \bar{\mathbf{P}}_k^* \mathbf{C}_{\mathbf{h}_k} \mathbf{C}_{\mathbf{r}_p}) \quad (18)$$

where the  $((u-1)M+m, (v-1)M+n)$ th element of  $\mathbf{C}_{\mathbf{r}_p}$  can be written as in (19) at the top of the page and the  $(m, (u-$

$1)M+n)$ th element of  $\mathbf{C}_{\mathbf{r}_p}$  can be written as

$$[\mathbf{C}_{\mathbf{r}_p}]_{m,(u-1)M+n} = (\rho K + 1) \left( \Omega(\text{Re}[\eta_{m,n,u}]) + j \Omega(\text{Im}[\eta_{m,n,u}]) \right). \quad (20)$$

*Proof:* See Appendix I. ■

The expression in (18) depends on: *i*) the specific data symbol vector  $\mathbf{x}$  through  $\mathbf{C}_{\mathbf{r}_p}$  in (20) and  $\eta_{m,n,u}$  in (17); and *ii*) on the pilot matrix  $\mathbf{P}$  through  $\mathbf{C}_{\mathbf{r}_p}$  in (19) and  $\zeta_{m,n,u,v}$  in (16) as well as  $\mathbf{C}_{\mathbf{r}_p}$  in (20) and  $\eta_{m,n,u}$  in (17). The important practical aspect is that the expected value of the soft-estimated symbol of UE  $k$  also depends on the specific data symbols transmitted by the interfering UEs. To simplify the notation in the rest of the paper, we omit the dependence on  $\mathbf{x}$  and  $\mathbf{P}$  and use the notation  $\mathbf{E}_k^{(\text{MRC})}$ .

Considering  $K = 2$  UEs, the soft-estimated symbols of UE 1 for each  $x_1 = s_{l_1} \in \mathcal{S}$  are generated and plotted along with their expected values in Fig. 1 while the transmit data symbol of the interfering UE is fixed to  $x_2 = \frac{1}{\sqrt{10}}(-1 + j)$ . Two SNR values are considered, i.e.,  $\rho = 0$  dB (Fig. 1a) and  $\rho = 20$  dB (Fig. 1b). Here, the soft-estimated symbols (black markers) originate from independent channel and AWGN realizations. We observe that, for each  $x_1 = s_{l_1} \in \mathcal{S}$ , the generated soft-estimated symbols are centered around the expected values obtained in (18) (red markers). In Fig. 1b, we further notice that the soft-estimated symbols and their expected values resulting from the data symbols with the same phase, i.e.,  $\frac{1}{\sqrt{10}}(\pm 1 \pm j)$  and  $\frac{1}{\sqrt{10}}(\pm 3 \pm 3j)$ , are almost overlapping due to the high SNR. This behavior, which was observed and analyzed in [17] for the single-UE case, implies that the amplitude information cannot be recovered at very high SNR. In general, the combination of 1-bit quantized chan-

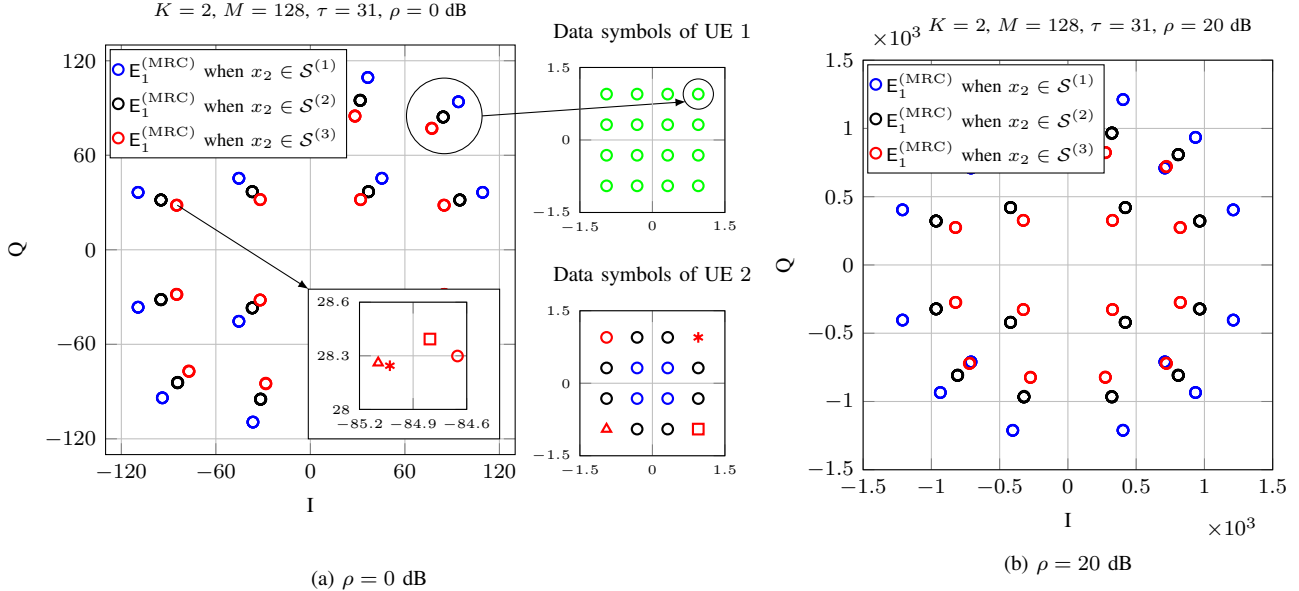


Fig. 2. Expected values of the soft-estimated symbols of UE 1 when UE 2 transmits all the possible data symbols; the MRC receiver is adopted at the BS.

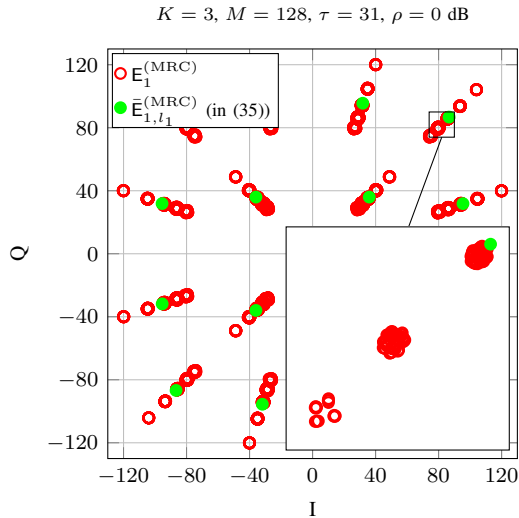


Fig. 3. Expected values of the soft-estimated symbols (red markers) and their mean values for UE 1 (green markers) when UE 2 and UE 3 transmit all the possible data symbols from  $\mathcal{S}$ ; the MRC receiver is adopted at the BS.

nel estimation and uplink data transmission produces a clear distortion in the transmit constellation, which directly depends on the SNR. Considering again  $K = 2$  UEs, Fig. 2 depicts the expected values of the soft-estimated symbols of UE 1 when both UEs transmit all the possible data symbols. As in Fig. 1, two SNR values are considered, i.e.,  $\rho = 0$  dB (Fig. 2a) and  $\rho = 20$  dB (Fig. 2b). The possible data symbols transmitted by UE 1 and UE 2 are also shown. For UE 2, the data symbols in the 16-QAM constellation with different amplitudes, i.e.,  $\mathcal{S}^{(1)} \triangleq \frac{1}{\sqrt{10}}\{\pm 1 \pm j\}$ ,  $\mathcal{S}^{(2)} \triangleq \frac{1}{\sqrt{10}}\{\pm 1 \pm 3j, \pm 3 \pm 1j\}$ , and  $\mathcal{S}^{(3)} \triangleq \frac{1}{\sqrt{10}}\{\pm 3 \pm 3j\}$ , are indicated with different colors, i.e., blue, black, and red, respectively. Each red marker shown in the zoomed part in the bottom-right corner corresponds to a specific data symbol in  $\mathcal{S}^{(3)}$ . In Fig. 2, there are  $16^2 = 256$

distinct pairs of data symbols transmitted by the two UEs, each corresponding to a different value of  $E_1^{(\text{MRC})}$  in (18). However, only  $3 \times 16 = 48$  points can be clearly distinguished, which implies that there is significant overlap among many of the 256 values of  $E_1^{(\text{MRC})}$ . This stems from the fact that, for a given  $x_1 = s_{l_1} \in \mathcal{S}$ , the data symbols with the same amplitude transmitted by UE 2 produce nearly the same value of  $E_1^{(\text{MRC})}$ . For this reason, the values of  $E_1^{(\text{MRC})}$  are shown in blue, black, and red when  $x_2 \in \mathcal{S}^{(1)}$ ,  $x_2 \in \mathcal{S}^{(2)}$ , and  $x_2 \in \mathcal{S}^{(3)}$ , respectively. To assess the impact of the SNR, we notice that, with  $\rho = 0$  dB (Fig. 2a), all the groups of points are well separated. In contrast, with  $\rho = 20$  dB (Fig. 2b), the groups of points corresponding to  $x_1, x_2 \in \mathcal{S}^{(1)}$  roughly overlap with those corresponding to  $x_1, x_2 \in \mathcal{S}^{(3)}$ . This occurs because  $x_1, x_2 \in \mathcal{S}^{(1)}$  have the smallest amplitude and are thus sensitive to the quantization distortion, which dominates at very high SNR.

Fig. 3 considers a similar setup but with  $K = 3$  UEs. Here, there are  $16^3 = 4096$  distinct triplets of data symbols transmitted by the three UEs, each corresponding to a different value of  $E_1^{(\text{MRC})}$  in (18). As in the case of  $K = 2$  UEs shown in Fig. 2, for a given  $x_1 = s_{l_1} \in \mathcal{S}$ , the data symbols with the same amplitude transmitted by UE 2 and UE 3 produce nearly the same value of  $E_1^{(\text{MRC})}$ . Interestingly, the dispersion of such values reduces as the pilot length increases since the channel estimates become more accurate. Note that the green markers in Fig. 3 represent the average of the expected values of the soft-estimated symbols of UE 1 corresponding to a specific transmitted data symbol, as defined in (35). These average values will be utilized in one of the data detection strategies presented in Section V-A.

#### B. Expected Values of the Soft-Estimated Symbols with ZF and MMSE

We now assume that a conventional ZF or MMSE receiver is adopted at the BS. Let  $\mathbf{v}_k^{(\text{ZF})}$  and  $\mathbf{v}_k^{(\text{MMSE})}$  denote the

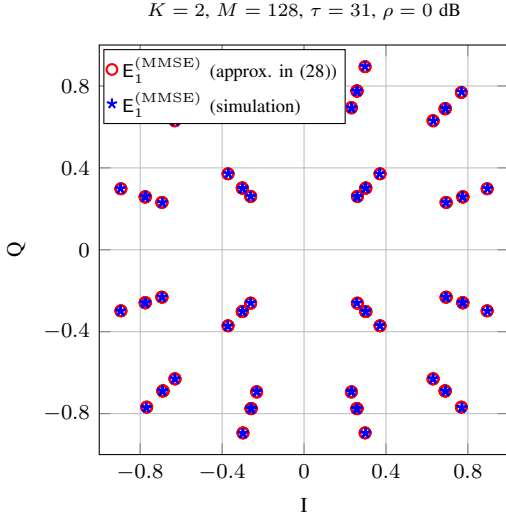


Fig. 4. Expected values of the soft-estimated symbols of UE 1 when UE 2 transmits all the possible data symbols; the MMSE receiver is adopted at the BS.

$k$ th columns of the ZF and MMSE receiver matrices given in (12) and (13), respectively. Then, the soft-estimated symbol of UE  $k$  can be expressed as  $\hat{x}_k^{(\text{ZF})} = (\mathbf{v}_k^{(\text{ZF})})^H \mathbf{r}$  or  $\hat{x}_k^{(\text{MMSE})} = (\mathbf{v}_k^{(\text{MMSE})})^H \mathbf{r}$  with the ZF and MMSE receiver, respectively. Thus, the expected value of the soft-estimated symbol of UE  $k$  for a given data symbol vector  $\mathbf{x}$  is given by

$$\mathbb{E}_k^{(\text{ZF})} \triangleq \mathbb{E}_{\mathbf{H}, \mathbf{z}, \mathbf{z}_p} [\hat{x}_k^{(\text{ZF})}], \quad (21)$$

$$\mathbb{E}_k^{(\text{MMSE})} \triangleq \mathbb{E}_{\mathbf{H}, \mathbf{z}, \mathbf{z}_p} [\hat{x}_k^{(\text{MMSE})}] \quad (22)$$

with the ZF and MMSE receiver, respectively.

In the following lemma, we analyze the asymptotic orthogonality of the channel estimates of two independent UEs obtained with the BLMMSE estimator. This result will be used to derive closed-form approximations of (21) and (22).

**Lemma 1.** *The channel estimates of two UEs  $k$  and  $k'$  obtained as in (7) are asymptotically orthogonal, i.e.,*

$$\frac{\hat{\mathbf{h}}_k^H \hat{\mathbf{h}}_{k'}}{\sqrt{\mathbb{E}[\|\hat{\mathbf{h}}_k\|^2]} \sqrt{\mathbb{E}[\|\hat{\mathbf{h}}_{k'}\|^2]}} \rightarrow 0 \quad \text{almost surely as } M \rightarrow \infty \quad (23)$$

if  $\mathbf{P}$  is chosen such that  $\mathbf{P}\mathbf{P}^H$  is circulant. However, (23) does not hold in general.

*Proof:* See Appendix II. ■

According to Lemma 1, as  $M \rightarrow \infty$ , the normalized inner product between  $\hat{\mathbf{h}}_k^H$  and  $\hat{\mathbf{h}}_{k'}$  tends to its expected value, but this is generally not zero due to a bias in the channel estimation with 1-bit ADCs (even in the presence of orthogonal pilots). If  $\mathbf{P}$  is chosen such that  $\mathbf{P}\mathbf{P}^H$  is circulant, as in the case of discrete Fourier transform (DFT) pilot matrix, then the expected value is zero. In this case, the asymptotic orthogonality between the channel estimates is equivalent to the asymptotically favorable propagation property of massive MIMO channels [20, Sec. 2.5.2].

From Lemma 1, when  $M$  is large, we have  $\frac{\hat{\mathbf{H}}^H \hat{\mathbf{H}}}{M} \approx \text{diag}([\frac{\|\hat{\mathbf{h}}_1\|^2}{M}, \dots, \frac{\|\hat{\mathbf{h}}_K\|^2}{M}])$  and thus we can write  $\mathbf{v}_k^{(\text{ZF})} \approx$

$\frac{\hat{\mathbf{h}}_k}{\|\hat{\mathbf{h}}_k\|^2}$ . Hence, (21) can be approximated as

$$\mathbb{E}_k^{(\text{ZF})} \approx \mathbb{E}_{\mathbf{H}, \mathbf{z}, \mathbf{z}_p} \left[ \frac{\hat{\mathbf{h}}_k^H \mathbf{r}}{\|\hat{\mathbf{h}}_k\|^2} \right] \approx \frac{\mathbb{E}_k^{(\text{MRC})}}{\mathbb{E}[\|\hat{\mathbf{h}}_k\|^2]} \quad (24)$$

with

$$\mathbb{E}[\|\hat{\mathbf{h}}_k\|^2] = \rho \text{tr}(\mathbf{C}_{\mathbf{h}_k} \bar{\mathbf{P}}_k^T \mathbf{A}_p \mathbf{C}_{\mathbf{r}_p}^{-1} \mathbf{A}_p \bar{\mathbf{P}}_k^* \mathbf{C}_{\mathbf{h}_k}). \quad (25)$$

To derive a closed-form approximation of (22), we first apply the matrix inversion lemma to write  $(\rho \hat{\mathbf{H}} \hat{\mathbf{H}}^H + \mathbf{I}_M)^{-1} = \mathbf{B}_k^{-1} - \rho \frac{\mathbf{B}_k^{-1} \hat{\mathbf{h}}_k \hat{\mathbf{h}}_k^H \mathbf{B}_k^{-1}}{1 + \rho \hat{\mathbf{h}}_k^H \mathbf{B}_k^{-1} \hat{\mathbf{h}}_k}$ , with  $\mathbf{B}_k \triangleq \rho \hat{\mathbf{H}}_{-k} \hat{\mathbf{H}}_{-k}^H + \mathbf{I}_M \in \mathbb{C}^{M \times M}$  and  $\hat{\mathbf{H}}_{-k} \triangleq [\hat{\mathbf{h}}_1, \dots, \hat{\mathbf{h}}_{k-1}, \hat{\mathbf{h}}_{k+1}, \dots, \hat{\mathbf{h}}_K] \in \mathbb{C}^{M \times (K-1)}$ . For simplicity and without loss of generality, let us consider the case of  $K = 2$  UEs and express the soft-estimated symbol of UE 1 as

$$\hat{x}_1^{(\text{MMSE})} = \hat{\mathbf{h}}_1^H \mathbf{B}_1^{-1} \mathbf{r} - \rho \hat{\mathbf{h}}_1^H \frac{\mathbf{B}_1^{-1} \hat{\mathbf{h}}_1 \hat{\mathbf{h}}_1^H \mathbf{B}_1^{-1}}{1 + \rho \hat{\mathbf{h}}_1^H \mathbf{B}_1^{-1} \hat{\mathbf{h}}_1} \mathbf{r}. \quad (26)$$

From Lemma 1, when  $M$  is large, we have

$$\hat{\mathbf{h}}_1^H \mathbf{B}_1^{-1} = \hat{\mathbf{h}}_1^H - \rho \hat{\mathbf{h}}_1^H \frac{\hat{\mathbf{h}}_2 \hat{\mathbf{h}}_2^H}{1 + \rho \|\hat{\mathbf{h}}_2\|^2} \approx \hat{\mathbf{h}}_1^H. \quad (27)$$

Finally, (22) can be approximated by plugging (27) into (26), which yields

$$\mathbb{E}_k^{(\text{MMSE})} \approx \mathbb{E}_{\mathbf{H}, \mathbf{z}, \mathbf{z}_p} \left[ \frac{\hat{\mathbf{h}}_k^H \mathbf{r}}{1 + \rho \|\hat{\mathbf{h}}_k\|^2} \right] \approx \frac{\mathbb{E}_k^{(\text{MRC})}}{1 + \rho \mathbb{E}[\|\hat{\mathbf{h}}_k\|^2]}. \quad (28)$$

From (24) and (28), it is straightforward to observe that the expected values of the soft-estimated symbols obtained with the ZF and MMSE receivers asymptotically correspond to scaled versions of their MRC counterparts. Considering  $K = 2$  UEs, Fig. 4 plots the expected values of the soft-estimated symbols of UE 1 when the MMSE receiver is adopted at the BS. We notice that the closed-form approximation in (28) coincides with the Monte Carlo simulation even for a moderate number of antennas (i.e.,  $M = 128$ ). In general, this approximation is accurate when  $\frac{M}{K}$  is sufficiently large.

#### IV. RECEIVER DESIGN

In the previous section, the receiver matrix was obtained by plugging the channel estimates (obtained with 1-bit ADCs) into the conventional MRC, ZF, and MMSE receiver structures. This type of receiver design, which is widely adopted in the literature on low-resolution massive MIMO [6], is inherited from infinite-resolution systems and thus ignores the non-linear effects of the low-resolution ADCs. Recently, a Busgang-based MMSE receiver for 1-bit ADCs was proposed in [14]. However, this receiver is designed under the assumption that the received signal in (8) is approximately Gaussian, which does not hold for a small-to-moderate number of UEs. Consequently, it overlooks the distorted shape of the transmit constellation due to the 1-bit ADCs, which is instead captured by the expected values of the soft-estimated symbols derived in Section III. Therefore, we propose a new receiver design that exploits these expected values of the soft-estimated symbols.

We begin by formulating the receiver design problem as

$$\mathbf{V}^* = \underset{\mathbf{V}}{\text{argmin}} \mathbb{E}_{\mathbf{x}, \mathbf{z}} \left[ \|\mathbf{V}^H \mathbf{r} - \mathbb{E}_{\mathbf{H}, \mathbf{z}, \mathbf{z}_p} [\mathbf{V}^H \mathbf{r} | \mathbf{x}]\|^2 \right] \quad (29)$$



where  $\mathbb{E}_{\mathbf{x}}[\cdot]$  is a discrete expectation over the  $L^K$  possible data symbol vectors. The problem in (29) aims at deriving a receiver, termed as *linear minimum mean dispersion* (LMMD) receiver, which minimizes the mean dispersion of the soft-estimated symbols (outer expectation) around their expected values (inner expectation). To make the formulation more tractable, we impose a conventional receiver structure that fixes the points around which the mean dispersion of the soft-estimated symbols is minimized. In this regard, we know from Section III-B that the expected values of the soft-estimated symbols for the MRC, ZF, and MMSE receivers are asymptotically the same up to a scaling. Therefore, we impose the MRC receiver in the inner expectation, so that (29) can be reformulated as

$$\mathbf{V}^{(\text{LMMD})} = \underset{\mathbf{V}}{\operatorname{argmin}} \mathbb{E}_{\mathbf{x}, \mathbf{z}} \left[ \left\| \mathbf{V}^H \mathbf{r} - \mathbb{E}_{\mathbf{H}, \mathbf{z}, \mathbf{z}_p} [\hat{\mathbf{H}}^H \mathbf{r} | \mathbf{x}] \right\|^2 \right]. \quad (30)$$

Finally, after some manipulations, the LMMD receiver can be obtained by setting the derivative of the objective of (30) to zero, which yields

$$\mathbf{V}^{(\text{LMMD})} = \frac{\sqrt{\rho}}{L^K} \mathbf{C}_r^\dagger \sum_{\mathbf{x} \in \mathcal{S}^K} \mathbf{G}(\mathbf{x}) \hat{\mathbf{H}} \mathbf{x} \mathbf{e}(\mathbf{x})^H \quad (31)$$

with

$$\mathbf{e}(\mathbf{x}) \triangleq \mathbb{E}_{\mathbf{H}, \mathbf{z}, \mathbf{z}_p} [\hat{\mathbf{H}}^H \mathbf{r} | \mathbf{x}] = [\mathbf{E}_1^{(\text{MRC})}, \dots, \mathbf{E}_K^{(\text{MRC})}]^T \in \mathbb{C}^K \quad (32)$$

where  $\mathbf{E}_k^{(\text{MRC})}$  is given in (18). Furthermore,  $\mathbf{C}_r \triangleq \mathbb{E}_{\mathbf{x}, \mathbf{z}} [\mathbf{r} \mathbf{r}^H] \in \mathbb{C}^{M \times M}$  and

$$\mathbf{G}(\mathbf{x}) = \mathbf{C}_{\mathbf{y}|\mathbf{x}}^H \mathbf{C}_{\mathbf{y}|\mathbf{x}}^{-1} \in \mathbb{C}^{M \times M} \quad (33)$$

is the Busgang gain matrix, with  $\mathbf{C}_{\mathbf{y}|\mathbf{x}} \triangleq \mathbb{E}_{\mathbf{z}} [\mathbf{y} \mathbf{y}^H | \mathbf{x}] \in \mathbb{C}^{M \times M}$  and  $\mathbf{C}_{\mathbf{y}^r|\mathbf{x}} \triangleq \mathbb{E}_{\mathbf{z}} [\mathbf{y}^r \mathbf{y}^r{}^H | \mathbf{x}] \in \mathbb{C}^{M \times M}$ . The detailed derivations are provided in Appendix III. Note that the channel estimation error with 1-bit ADCs increases at high SNR [17]. Hence, imperfect CSI can significantly deteriorate the performance of the LMMD receiver when the SNR is set too high. Nonetheless, it is shown in Section VI that the LMMD receiver significantly outperforms the conventional receivers at the optimal SNR, which can be achieved via power control.

## V. DATA DETECTION STRATEGIES

In this section, we exploit the mutually dependent expected values of the soft-estimated symbols described in Section III and the minimum distance criterion to map each soft-estimated symbol in (10) to one of the possible data symbols in  $\mathcal{S}$ . Note that the following data detection strategies are general and can be applied to any receiver structure described in Sections III and IV. In this regard, we use  $\mathbf{E}_k$  to denote the expected value of the soft-estimated symbol of UE  $k$  obtained by any of the conventional receivers, i.e., MRC, ZF, and MMSE. In the following, we use  $l_k^* \in \{1, \dots, L\}$  to denote the index of the detected data symbol of UE  $k$ .

### A. Single-UE Data Detection Strategies

Here, we consider the soft-estimated symbols and their expected values of each intended UE separately. In this respect, we present three single-UE data detection strategies (SUD): 1) exhaustive, 2) heuristic, and 3) genie-aided data detection.

**Exhaustive SUD (E-SUD).** This strategy uses the statistical information (e.g., covariance matrices) of the interfering UEs

to detect the data symbol of the target UE. Let  $\mathcal{E}_k \triangleq \{\mathbf{E}_k, \forall \mathbf{x} \in \mathcal{S}^K\}$  denote the set of the expected values of the soft-estimated symbols for UE  $k$  obtained from all the possible data symbol vectors, with  $|\mathcal{E}_k| = L^K$ . The soft-estimated symbol of UE  $k$  is mapped to one of the elements in  $\mathcal{E}_k$  as

$$\mathbf{E}_k^* = \underset{\mathbf{E}_k \in \mathcal{E}_k}{\operatorname{argmin}} |\hat{x}_k - \mathbf{E}_k| \quad (34)$$

from which  $l_k^*$  is readily obtained. This strategy amounts to performing an exhaustive search over all the  $L^K$  possible values of  $\mathbf{E}_k$ . Hence, its complexity increases exponentially with  $K$ .

**Heuristic SUD (H-SUD).** This strategy considers the average of expected values of the soft-estimated symbols of the target UE over all the possible data symbols transmitted by the interfering UEs. Let  $\mathbf{x}_{-k} \triangleq [x_1, \dots, x_{k-1}, x_{k+1}, \dots, x_K]^T \in \mathbb{C}^{K-1}$  and let  $\mathcal{E}_{k, l_k} \triangleq \{\mathbf{E}_k : x_k = s_{l_k}, \forall \mathbf{x}_{-k} \in \mathcal{S}^{K-1}\} \subset \mathcal{E}_k$  be the set containing the elements in  $\mathcal{E}_k$  corresponding to  $x_k = s_{l_k}$ , with  $|\mathcal{E}_{k, l_k}| = L^{K-1}$ . Furthermore, let us define

$$\bar{\mathbf{E}}_{k, l_k} \triangleq \frac{1}{L^{K-1}} \sum_{t \in \mathcal{E}_{k, l_k}} t \quad (35)$$

which represents the average of expected values of the soft-estimated symbols of the target UE over all the possible data symbols transmitted by the interfering UEs (depicted by the green markers in Fig. 3). Then, the index of the detected data symbol of UE  $k$  is obtained as

$$l_k^* = \underset{l_k \in \{1, \dots, L\}}{\operatorname{argmin}} |\hat{x}_k - \bar{\mathbf{E}}_{k, l_k}|. \quad (36)$$

This strategy is a low-complexity, heuristic version of *E-SUD*, reducing the size of the search space from  $L^K$  to  $L$ .

**Genie-aided data detection.** This strategy assumes a genie ideally provides the data symbols transmitted by the interfering UEs to minimize the uncertainty in detecting the data symbol of the target UE. Hence, for UE  $k$ ,  $\mathbf{x}_{-k}$  is assumed to be perfectly known, which reduces the size of the search space from  $L^K$  to  $L$ . Evidently, this strategy is impractical and considered only to evaluate the impact of perfect knowledge of the data symbols transmitted by the interfering UEs on the data detection performance of the target UE.

### B. Enhanced Multi-UE Data Detection Strategies

*E-SUD* proposed in Section V-A maps each soft-estimated symbol of the target UE to one of the  $L^K$  expected values of the soft-estimated symbols based on the minimum distance criterion. This method is impractical since it performs an exhaustive search over the set of expected values of the soft-estimated symbols corresponding to the target UE resulting from all the possible data symbol vectors, whose size grows exponentially with the number of UEs. In addition, it does not take advantage of the interdependence among the soft-estimated symbols of the interfering UEs as it treats each UE individually. Hence, we present two data detection strategies that exploit this interdependence: 1) joint data detection (JD) and 2)  $N$ -point joint data detection ( $N$ -JD). We compare our proposed data detection strategies with RML proposed in [14]. RML is a reformulated ML detection problem that approximates the cumulative distribution function of a Gaussian random variable with a sigmoid function, thereby circumventing

the non-robustness issue of conventional ML detection [14]. The corresponding formulation and discussion are reproduced for convenience in Appendix IV. On the other hand, the JD and  $N$ -JD strategies use the minimum distance criterion to map each soft-estimated symbol in (10) to one of the expected values of the soft-estimated symbols as described in Section III, and thus to one of the possible data symbols in  $\mathcal{S}$ .

**Joint data detection (JD).** This strategy takes the expected values of the soft-estimated symbols of the interfering UEs into account, which leads to enhanced multi-UE data detection of the target UE. Regardless of which receiver is adopted at the BS, let  $\mathbf{E}_{k,l_k}(\mathbf{x}_{-k})$  denote the expected value of the soft-estimated symbol of UE  $k$  for  $x_k = s_{l_k}$  specific to each transmit vector of the interfering UEs  $\mathbf{x}_{-k} \triangleq [x_1, \dots, x_{k-1}, x_{k+1}, \dots, x_K]^T \in \mathbb{C}^{K-1}$ . For simplicity and without loss of generality, we consider  $K = 2$  in the following. Let  $\mathbf{E}_{l_1,l_2} \triangleq [\mathbf{E}_{1,l_1}(s_{l_2}), \mathbf{E}_{2,l_2}(s_{l_1})]^T$  denote the vector containing the expected values of the soft-estimated symbols of the two UEs when  $x_1 = s_{l_1}$  and  $x_2 = s_{l_2}$ . Let  $\mathcal{E} \triangleq \{\mathbf{E}_{l_1,l_2}, \forall (s_{l_1}, s_{l_2}) \in \mathcal{S}^2\}$  denote the set of vectors comprising the expected values of the soft-estimated symbols for both UEs resulting from all the possible data symbol vectors, with  $|\mathcal{E}| = L^2$ . The soft-estimated symbol vector  $\hat{\mathbf{x}}$  is mapped to one of the vectors  $\mathbf{E}_{l_1,l_2} \in \mathcal{E}$  as

$$\mathbf{E}^* = \underset{\mathbf{E}_{l_1,l_2} \in \mathcal{E}}{\operatorname{argmin}} \|\hat{\mathbf{x}} - \mathbf{E}_{l_1,l_2}\| \quad (37)$$

from which  $\{l_k^*\}_{k=1}^K$  can be extracted. In general, this strategy amounts to performing an exhaustive search over all the  $L^K$  possible vectors  $\mathbf{E}_{l_1,\dots,l_K} \triangleq [\mathbf{E}_{1,l_1}(\mathbf{x}_{-1}), \dots, \mathbf{E}_{K,l_K}(\mathbf{x}_{-K})]^T$ . Hence, the complexity of this strategy increases exponentially with  $K$  as for E-SUD.

**$N$ -point joint data detection ( $N$ -JD).** This strategy can be seen as a low-complexity variant of JD. First, we consider the  $N \leq L$  values of  $\bar{\mathbf{E}}_{k,l_k}$  in (35) that are closest to each UE's soft-estimated symbol  $\hat{x}_k$ . In this regard, let  $\mathcal{S}'_k = \{s_{l_k}^{(1)}, s_{l_k}^{(2)}, \dots, s_{l_k}^{(N)}\}$  represent the set containing the detected data symbols of UE  $k$ , where  $s_{l_k}^{(i)}$  denotes the detected data symbol corresponding to the  $i$ th closest value of  $\bar{\mathbf{E}}_{k,l_k}$  to each soft-estimated symbol of UE  $k$ . From  $\mathbf{E}_{l_1,\dots,l_K}$ , which is defined for JD, let  $\mathcal{E}_{N\text{-JD}} \triangleq \{\mathbf{E}_{l_1,\dots,l_K}, \forall (s_{l_1}, \dots, s_{l_K}) \in \prod_{k=1}^K \mathcal{S}'_k\}$  denote the restricted set of vectors  $\mathbf{E}_{l_1,\dots,l_K}$  resulting from the data symbol vectors belonging to the Cartesian product of  $\mathcal{S}'_k$  across all the UEs, with  $|\mathcal{E}_{N\text{-JD}}| = N^K$ . The soft-estimated symbol vector  $\hat{\mathbf{x}}$  is mapped to one of the vectors  $\mathbf{E}_{l_1,\dots,l_K} \in \mathcal{E}_{N\text{-JD}}$  as

$$\mathbf{E}^* = \underset{\mathbf{E}_{l_1,\dots,l_K} \in \mathcal{E}_{N\text{-JD}}}{\operatorname{argmin}} \|\hat{\mathbf{x}} - \mathbf{E}_{l_1,\dots,l_K}\| \quad (38)$$

from which  $\{l_k^*\}_{k=1}^K$  can be extracted. As a result, the size of the search space is  $N^K$ , which can be made considerably smaller compared with  $L^K$  of JD by adjusting the value of  $N$ .

### C. Computational Complexity Analysis

The computational complexity of all the data detection strategies is summarized in Table I. RML with NN search, which is described in [14], finds a set of  $N_{\text{NN}}$  data symbol

| Data detection strategy    | Computational complexity                               |
|----------------------------|--|
| RML with NN search [14]    | $\mathcal{O}(N_{\text{NN}}K \max\{N_{\text{NN}}, M\})$ |
| JD                         | $\mathcal{O}(L^K)$                                     |
| $N$ -JD                    | $\mathcal{O}(N^K)$                                     |
| H-SUD                      | $\mathcal{O}(L)$                                       |
| E-SUD                      | $\mathcal{O}(L^K)$                                     |
| Genie-aided data detection | $\mathcal{O}(L)$                                       |

Table I. Computational complexity.

vectors in  $\mathcal{S}^K$  that are nearest to  $\hat{\mathbf{x}}$ . Then, RML with NN search only explores this smaller set for the final solution. In this regard, while the computational complexity of this method does not increase exponentially with the number of UEs, it depends on the number of BS antennas. This can be seen from the fact that  $\max\{N_{\text{NN}}, M\} = M$ , where  $M$  is significantly large in the massive MIMO regime. Therefore, the complexity of RML with NN search is high. On the other hand, the computational complexity of the proposed JD is  $\mathcal{O}(L^K)$ , which can increase significantly with  $L$  and exponentially with  $K$ . Lastly,  $N$ -JD has the lowest computational complexity among the enhanced multi-UE data detection strategies as  $\mathcal{O}(N^K)$ . As discussed in Section V-B, while this complexity grows exponentially with  $K$ , the value of  $N$  is adjustable. Thus, the complexity of  $N$ -JD is substantially less than that of JD and remarkably less than the complexity of RML, particularly for small values of  $K$ .

## VI. NUMERICAL RESULTS AND DISCUSSION

In this section, we evaluate the impact of the different receivers (i.e., MRC, MMSE, and LMMD) and the data detection strategies described in Section V-B in terms of SER. We consider either  $K = 2$  or  $K = 3$  UEs and, unless otherwise stated, we assume that the BS is equipped with  $M = 128$  antennas. The channel covariance matrices are generated based on the one-ring channel model [21] with angular spread of  $30^\circ$  for each UE and angular separation of  $30^\circ$  between the UEs. All the UEs are subject to the same (normalized) pathloss, such that  $\operatorname{tr}(\mathbf{C}_{\mathbf{h}_k}) = M$ ,  $\forall k = 1, \dots, K$ ; unless otherwise stated, we consider  $\rho = 0$  dB. The orthogonal pilots used for the channel estimation described in Section II-A are constructed as Zadoff-Chu sequences, which are widely adopted in the 4G LTE and 5G NR standards [22]; unless otherwise stated, we fix  $\tau = 31$ . All the SER results are obtained by averaging over  $4 \times 10^3$  independent channel and AWGN realizations and taking all the possible data symbols into account.

Considering  $K = 2$ , Fig. 5 plots the SER as a function of the SNR obtained with different receivers described in Section III and IV, and JD demonstrated in V-B. We observe in Fig. 5 that all the SER curves feature an optimal SNR operating point: at low SNR, the AWGN is dominant; at high SNR, the soft-estimated symbols corresponding to the data symbols with the same phase are hardly distinguishable. In between these regimes, the right level of AWGN produces a proper scrambling of the 1-bit quantized signals at the  $M$  antennas. Remarkably, there is a significant gain with MMSE compared with MRC. As demonstrated in Section V-A, these expected values can be asymptotically obtained with simple scaling of their MRC counterparts in (18). Here, we note that Lemma 1 leading to (22) does not hold with Zadoff-Chu pilots, but



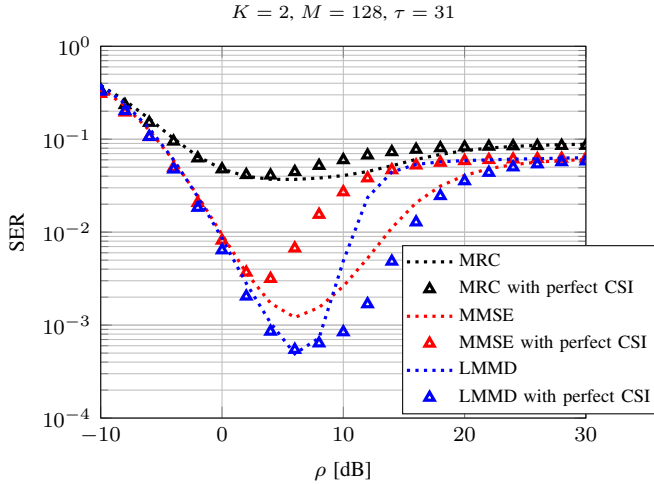


Fig. 5. SER versus SNR obtained with JD and different receivers.

nonetheless (23) tends to a very small value. As a result, the SER gain with the MMSE receiver is not due to their expected values but the reduced dispersion of the soft-estimated symbols around them. Furthermore, we can see from Fig. 5 that the SER obtained with MRC and MMSE receivers with imperfect CSI are better than that with perfect CSI. This is because these receivers with perfect CSI are not adopted for 1-bit ADCs; as a consequence, they ignore the quantization distortion while the channel estimate takes into account the inherent scaling ambiguity in the observed data, as mentioned in [14].

The SER curves obtained with the LMMD receiver, both with perfect and imperfect CSI, are also shown in Fig. 5. We observe in Fig. 5 that the LMMD receiver with perfect CSI outperforms all other receivers. This is because the LMMD receiver aims to minimize the mean dispersion of the soft-estimated symbols around the values of  $e(\mathbf{x})$ . However, in the case of imperfect CSI, the LMMD receiver gets worse than MMSE as  $\rho$  grows. In fact, while the criterion for the LMMD receiver design is to minimize the mean dispersion, it cannot always be the best choice for each of the expected values given in (18); otherwise, we would need a symbol-based receiver. In other words, the LMMD receiver cannot minimize the dispersion around each of these expected values since the groups of the soft-estimated symbols resulting from the data symbols with the same phase get closer at high SNR, as discussed in Section III.

Considering  $K = 2$  UEs, Fig. 6 plots the SER as a function of the SNR obtained with all the data detection strategies described in Section V when the LMMD receiver is adopted at the BS. For comparison, we also include the RML method presented in [14]. In order to achieve the maximum performance of RML, we consider a full search over all the possible data symbol vectors  $\mathbf{x}$ . Fig. 6 shows that E-SUD is better than H-SUD since the latter considers the values of  $\bar{E}_{k,l,k}$ , which is defined in (35). We note that H-SUD is the same as  $N$ -JD with  $N = 1$ . As in Fig. 6, the genie-aided data detection outperforms JD. This is because JD suffers from error propagation between the detected data symbols of the UEs, particularly at high SNR, whereas the genie-aided

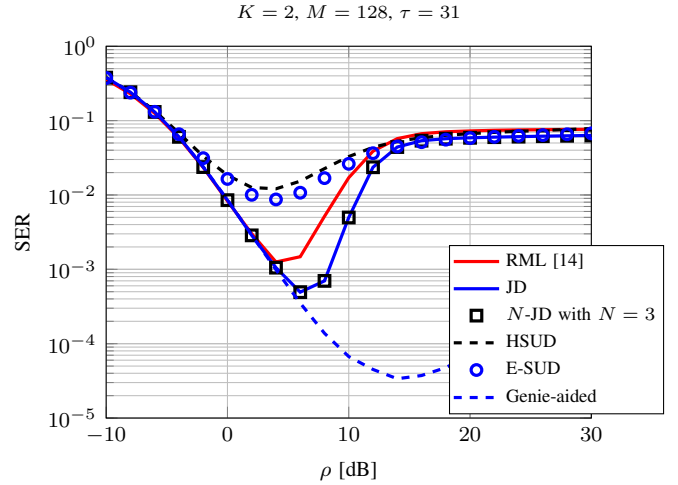


Fig. 6. SER versus SNR obtained with different data detection strategies and the LMMD receiver.

data detection assumes perfect knowledge of the data symbols transmitted by the interfering UEs, as detailed in Section V-A. However, the genie-aided data detection is impractical and considered only to evaluate the impact of perfect knowledge of the data symbols transmitted by the interfering UEs on the data detection performance of the target UE. Remarkably, we can see in Fig. 6 that JD and  $N$ -JD with  $N = 3$  provide a significant boost in comparison with E-SUD. This means that taking advantage of the interdependence among the soft-estimated symbols of the interfering UEs gives a notable gain over the data detection strategies that treat each UE individually. Lastly, Fig. 6 demonstrates that while RML performs similarly to the proposed JD and  $N$ -JD strategies at low SNR, its performance deteriorates at moderate-to-high SNR. As the SNR increases, the data symbols with the same phase produce nearly the same 1-bit quantized signals. This makes them hard to distinguish since the objective function in (75) remains nearly the same at high SNR. Therefore, while RML is designed to be robust against the channel estimation error, it does not account for these similarities and thus becomes inferior to JD and  $N$ -JD.

Considering  $K = 2$  UEs, Fig. 7a illustrates that  $N$ -JD exhibits the same performance with respect to JD with  $N = 3$ . This is because, with  $K = 2$ , there is significant overlap among many of the 256 expected values of the soft-estimated symbols. In addition, since there are three different amplitude levels in the 16-QAM constellation, only  $3 \times 16$  expected values can be clearly distinguished (see Fig. 2). Fig. 7b extends the insights of Fig. 7a to the case of  $K = 3$ . Here, there are  $16^3 = 4096$  different triplets of data symbols transmitted by the three UEs, each corresponding to a different expected value (see Fig. 3). Remarkably,  $N$ -JD with  $N = 3$  nearly matches JD while its computational complexity is only three times more than the case of  $K = 2$  UEs.

Considering  $K = 2$  UEs and the data detection strategies depicted in Fig. 7a, Fig. 8 illustrates the impact of the number of BS antennas  $M$  on the minimum achievable SER over the SNR  $\rho$ . We observe that the minimum SER monotonically decreases as  $M$  grows since higher granularity in the antenna domain contributes to a proper scrambling of a larger number

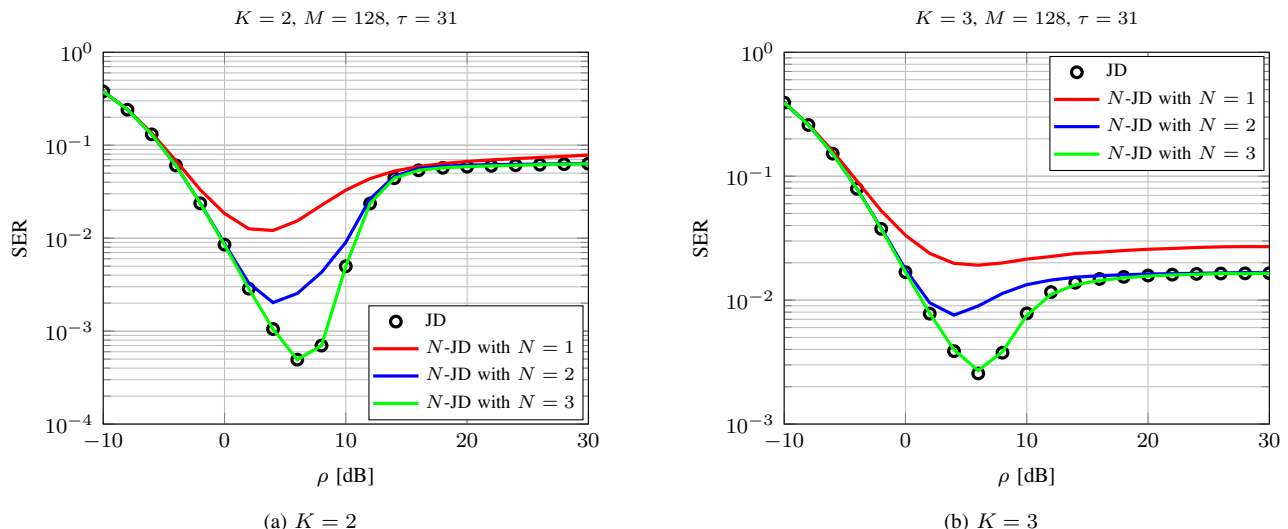


Fig. 7. SER versus SNR obtained with JD and  $N$ -JD (both with the LMMD receiver).

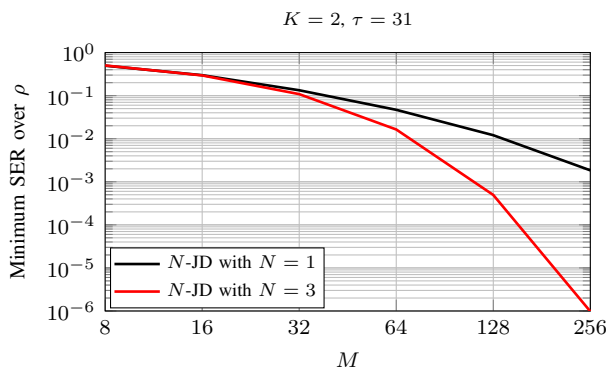


Fig. 8. Minimum SER versus number of BS antennas obtained with  $N$ -JD and the LMMD receiver.

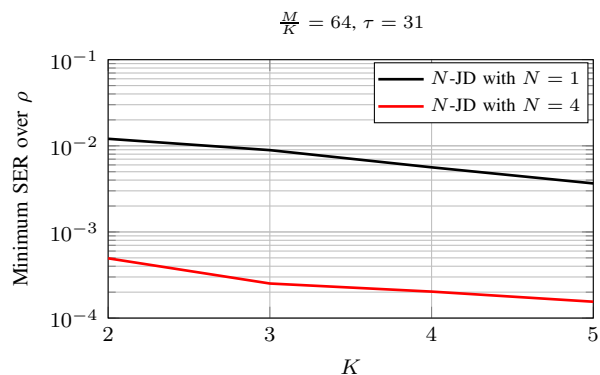


Fig. 9. Minimum SER versus number of UEs obtained with  $N$ -JD and the LMMD receiver.

of the 1-bit quantized signals, thereby reducing the dispersion of the soft-estimated symbols in the vicinity of their expected values. For too small values of  $M$ , the gain from JD vanishes because the candidate points within each group of the expected values of the soft-estimated symbols become indistinguishable due to prohibitively large quantization distortion. Fig. 9 plots the minimum SER over the SNR  $\rho$  against the number of UEs for  $N$ -JD. It can be readily seen that the gap in Fig. 9 between  $N$ -JD with  $N = 4$  and  $N = 1$  remains the same as expected, while the SER decreases for both cases as  $M$  increases.

## VII. CONCLUSIONS

Considering a multi-UE setting with correlated Rayleigh fading, we investigated the uplink data detection in a single-cell massive MIMO system with 1-bit ADCs. We first characterized the expected values of the soft estimated symbols, which effectively capture the distortion in the transmit constellation due to the 1-bit quantization during both the channel estimation and the uplink data transmission. In our analysis, we considered the conventional receivers such as MRC, ZF, and MMSE. Additionally, we designed a *linear minimum mean dispersion* (LMMD) receiver tailored for the data detection with 1-bit ADCs, which exploits the expected values of the soft-estimated symbols. Then, we proposed a joint data detec-

tion (JD) strategy that exploits the interdependence among the soft-estimated symbols of the interfering UEs, along with its low-complexity variant. Numerical results examining the SER showed that MMSE exhibits a considerable performance gain over MRC, whereas the proposed LMMD receiver significantly outperforms all the conventional receivers. Lastly, the proposed JD and its low-complexity variant provided a significant boost in comparison with the single-UE data detection.

## APPENDIX I PROOF OF THEOREM 1

Considering (7) and (9), for a given data symbol vector  $\mathbf{x}$ , the expected value of the soft-estimated symbol of UE  $k$  obtained with the MRC receiver is  $\mathbb{E}_k^{(\text{MRC})} = \mathbb{E}[\hat{\mathbf{h}}_k^H \mathbf{r}]$  given by (18). Next, we derive closed-form expressions of  $\mathbf{C}_{\text{rrp}}$  and  $\mathbf{C}_{\text{rp}}$  defined in Sections III-A and II-A, respectively. To this end, let  $\bar{\mathbf{h}}_k \triangleq \mathbf{C}_{\mathbf{h}_k}^{-\frac{1}{2}} \mathbf{h}_k$ , and let  $\bar{h}_{i,k}$  and  $h_{i,k}$  denote the  $i$ th

element of  $\bar{\mathbf{h}}_k$  and  $\mathbf{h}_k$ , respectively, with

$$h_{m,k} = \sum_{i=1}^M [\mathbf{C}_{\mathbf{h}_k}^{\frac{1}{2}}]_{m,i} \bar{h}_{i,k}, \quad (39)$$

$$\begin{aligned} \text{Re}[h_{m,k}] &= \sum_{i=1}^M \left( \text{Re}[[\mathbf{C}_{\mathbf{h}_k}^{\frac{1}{2}}]_{m,i}] \text{Re}[\bar{h}_{i,k}] \right. \\ &\quad \left. - \text{Im}[[\mathbf{C}_{\mathbf{h}_k}^{\frac{1}{2}}]_{m,i}] \text{Im}[\bar{h}_{i,k}] \right), \quad (40) \end{aligned}$$

$$\begin{aligned} \text{Im}[h_{m,k}] &= \sum_{i=1}^M \left( \text{Re}[[\mathbf{C}_{\mathbf{h}_k}^{\frac{1}{2}}]_{m,i}] \text{Im}[\bar{h}_{i,k}] \right. \\ &\quad \left. + \text{Im}[[\mathbf{C}_{\mathbf{h}_k}^{\frac{1}{2}}]_{m,i}] \text{Re}[\bar{h}_{i,k}] \right). \quad (41) \end{aligned}$$

Moreover, we introduce the following preliminary definitions:

$$\begin{aligned} A_{m,u} &\triangleq \text{sgn} \left( \sqrt{\rho} \sum_{k=1}^K \sum_{i=1}^M \left( \text{Re}[\bar{h}_{i,k}] \text{Re}[[\mathbf{C}_{\mathbf{h}_k}^{\frac{1}{2}}]_{m,i} P_{u,k}^*] \right. \right. \\ &\quad \left. \left. - \text{Im}[\bar{h}_{i,k}] \text{Im}[[\mathbf{C}_{\mathbf{h}_k}^{\frac{1}{2}}]_{m,i} P_{u,k}^*] \right) + \text{Re}[z_{P_{m,u}}] \right), \quad (42) \end{aligned}$$

$$\begin{aligned} B_{m,u} &\triangleq \text{sgn} \left( \sqrt{\rho} \sum_{k=1}^K \sum_{i=1}^M \left( \text{Re}[\bar{h}_{i,k}] \text{Im}[[\mathbf{C}_{\mathbf{h}_k}^{\frac{1}{2}}]_{m,i} P_{u,k}^*] \right. \right. \\ &\quad \left. \left. + \text{Im}[\bar{h}_{i,k}] \text{Re}[[\mathbf{C}_{\mathbf{h}_k}^{\frac{1}{2}}]_{m,i} P_{u,k}^*] \right) + \text{Im}[z_{P_{m,u}}] \right), \quad (43) \end{aligned}$$

$$\begin{aligned} a_m &\triangleq \text{sgn} \left( \sqrt{\rho} \sum_{k=1}^K \sum_{i=1}^M \left( \text{Re}[\bar{h}_{i,k}] \text{Re}[[\mathbf{C}_{\mathbf{h}_k}^{\frac{1}{2}}]_{m,i} x_k] \right. \right. \\ &\quad \left. \left. - \text{Im}[\bar{h}_{i,k}] \text{Im}[[\mathbf{C}_{\mathbf{h}_k}^{\frac{1}{2}}]_{m,i} x_k] \right) + \text{Re}[z_m] \right), \quad (44) \end{aligned}$$

$$\begin{aligned} b_m &\triangleq \text{sgn} \left( \sqrt{\rho} \sum_{k=1}^K \sum_{i=1}^M \left( \text{Re}[\bar{h}_{i,k}] \text{Im}[[\mathbf{C}_{\mathbf{h}_k}^{\frac{1}{2}}]_{m,i} x_k] \right. \right. \\ &\quad \left. \left. + \text{Im}[\bar{h}_{i,k}] \text{Re}[[\mathbf{C}_{\mathbf{h}_k}^{\frac{1}{2}}]_{m,i} x_k] \right) + \text{Im}[z_m] \right). \quad (45) \end{aligned}$$

The following proposition will be used in the derivations. The proof is based on [17, App. II] and is thus omitted.

**Proposition 1.** Let  $\zeta \sim \mathcal{N}(\mathbf{0}_N, \gamma \mathbf{I}_N)$ . For  $\mathbf{a}_1, \mathbf{a}_2 \in \mathbb{R}^N$ , we have

$$\mathbb{E}[\text{sgn}(\mathbf{a}_1^T \zeta) \text{sgn}(\mathbf{a}_2^T \zeta)] = \Omega \left( \frac{\mathbf{a}_1^T \mathbf{a}_2}{\|\mathbf{a}_1\| \|\mathbf{a}_2\|} \right). \quad (46)$$

We can write the  $(m, (u-1)M+n)$ th element of  $\mathbf{C}_{\text{rr}_p}$  as

$$\mathbb{E}[r_m r_{p,n,u}^*] = \frac{\rho K + 1}{2} \left( \mathbb{E}[(a_m + j b_m)(A_{n,u} - j B_{n,u})] \right) \quad (47)$$

$$= (\rho K + 1) (\mathbb{E}[a_m A_{n,u}] + j \mathbb{E}[b_m A_{n,u}]) \quad (48)$$

with  $\mathbb{E}[a_m A_{n,u}] = \mathbb{E}[b_m B_{n,u}]$  and  $\mathbb{E}[b_m A_{n,u}] = -\mathbb{E}[a_m B_{n,u}]$ . Hence, (48) is expressed as in (49) at the end of the document. For instance,  $\mathbb{E}[a_m A_{n,u}]$  in (50) can be obtained by plugging (51)–(53) at the end of the document into Proposition (1), which gives (54) at the end of the document. Finally, the expression in (20) readily follows.

Similarly, we can write the  $((u-1)M+m, (v-1)M+n)$ th

element of  $\mathbf{C}_{\text{r}_p}$  as

$$\begin{aligned} \mathbb{E}[r_{p,m,u} r_{p,n,v}^*] &= \frac{\rho K + 1}{2} (\mathbb{E}[A_{m,u} A_{n,v}] + \mathbb{E}[B_{m,u} B_{n,v}]) \\ &\quad - j \mathbb{E}[A_{m,u} B_{n,v}] + j \mathbb{E}[B_{m,u} A_{n,v}] \quad (55) \end{aligned}$$

with  $\mathbb{E}[A_{m,u} A_{n,v}] = \mathbb{E}[B_{m,u} B_{n,v}]$  and  $\mathbb{E}[A_{m,u} B_{n,v}] = -\mathbb{E}[B_{m,u} A_{n,v}]$ . The rest of the derivations follow similar steps as in (49)–(54), which finally yield the expression in (19).

## APPENDIX II PROOF OF LEMMA 1

The proof follows similar steps as the proof of the asymptotically favorable propagation of massive MIMO channels in [20, Sec. 2.5.2]. For a pair of channel estimates  $\hat{\mathbf{h}}_k$  and  $\hat{\mathbf{h}}_{k'}$ , with  $k \neq k'$ , asymptotic orthogonality holds if (23) is satisfied. According to the definitions in Section II-A, we use the Bussgang decomposition to rewrite  $\mathbf{r}_p$  in (4) as [5]

$$\mathbf{r}_p = \mathbf{A}_p \mathbf{y}_p + \mathbf{q}_p = \sqrt{\rho} \mathbf{A}_p \bar{\mathbf{P}}^* \mathbf{h} + \mathbf{A}_p \mathbf{z}_p + \mathbf{q}_p \quad (56)$$

where  $\mathbf{q}_p \in \mathbb{C}^{M\tau}$  is the quantization distortion vector that is uncorrelated with  $\mathbf{y}_p$ . Let  $\mathbf{n} \triangleq \mathbf{A}_p \mathbf{z}_p + \mathbf{q}_p \in \mathbb{C}^{M\tau}$  denote the effective noise with zero mean and covariance matrix

$$\mathbf{C}_n \triangleq \mathbb{E}[\mathbf{n}\mathbf{n}^H] = \mathbf{C}_{\text{r}_p} - \rho \mathbf{A}_p \bar{\mathbf{P}}^* \mathbf{C}_h \bar{\mathbf{P}}^T \mathbf{A}_p \in \mathbb{C}^{M\tau \times M\tau}. \quad (57)$$

In addition, let  $\mathbf{X}_k \triangleq \mathbf{C}_{\mathbf{h}_k} \bar{\mathbf{P}}_k^T \mathbf{A}_p \mathbf{C}_{\text{r}_p}^{-1} \in \mathbb{C}^{M \times M\tau}$ . From (7) and (25), we can write (58) (at the end of the document), with  $\bar{\mathbf{h}} \triangleq \mathbf{C}_h^{-\frac{1}{2}} \mathbf{h}$  and  $\bar{\mathbf{n}} \triangleq \mathbf{C}_n^{-\frac{1}{2}} \mathbf{n}$ , where the latter can be modeled as a  $\mathcal{CN}(\mathbf{0}_{M\tau}, \mathbf{I}_{M\tau})$  random vector as in [14]. From (25), we have  $\mathbb{E}[\|\hat{\mathbf{h}}_k\|^2] = \rho \text{tr}(\mathbf{X}_k \mathbf{C}_{\text{r}_p} \mathbf{X}_k^H)$  and, for a given  $M$  and average eigenvalue  $\beta_{\text{av}}$  of  $\mathbf{X}_k \mathbf{C}_{\text{r}_p} \mathbf{X}_k^H$ , it follows that  $\mathbb{E}[\|\hat{\mathbf{h}}_k\|^2] = M \rho \beta_{\text{av}}$ . For i.i.d. Rayleigh fading, (25) becomes

$$\mathbb{E}[\|\hat{\mathbf{h}}_k\|^2] = \frac{2\rho}{\pi(\rho K + 1)} \text{tr}((\mathbf{p}_k^T \Phi^{-1} \mathbf{p}_k^*) \otimes \mathbf{I}_M) \quad (60)$$

$$= M \frac{2\rho}{\pi(\rho K + 1)} \mathbf{p}_k^T \Phi^{-1} \mathbf{p}_k^* \quad (61)$$

with  $\mathbf{C}_{\text{r}_p} = (\rho K + 1) \Phi \otimes \mathbf{I}_M$  and where the  $(u, v)$ th element of  $\Phi \in \mathbb{C}^{\tau \times \tau}$  is given by

$$[\Phi]_{u,v} \triangleq \begin{cases} 1 & \text{if } u = v, \\ \Omega \left( \frac{\rho \sum_{k=1}^K \text{Re}[P_{u,k} P_{v,k}^*]}{\rho K + 1} \right) - j \Omega \left( \frac{\rho \sum_{k=1}^K \text{Im}[P_{u,k} P_{v,k}^*]}{\rho K + 1} \right) & \text{if } u \neq v. \end{cases} \quad (62)$$

Therefore, from (61),  $\mathbb{E}[\|\hat{\mathbf{h}}_k\|^2]$  increases linearly with  $M$ . Now, plugging (58) into (23) yields (63) at the end of the document. as  $M \rightarrow \infty$ , where the convergence holds based on [23, Thm. 3.7]. For i.i.d. Rayleigh fading, (63) becomes

$$(63) = \frac{\text{tr}(\mathbf{X}_k \mathbf{C}_{\text{r}_p} \mathbf{X}_{k'}^H)}{\sqrt{\text{tr}(\mathbf{X}_k \mathbf{C}_{\text{r}_p} \mathbf{X}_k^H) \text{tr}(\mathbf{X}_{k'} \mathbf{C}_{\text{r}_p} \mathbf{X}_{k'}^H)}} \quad (64)$$

$$= \frac{\text{tr}(\bar{\mathbf{P}}_k^T \mathbf{C}_{\text{r}_p}^{-1} \bar{\mathbf{P}}_{k'}^*)}{\sqrt{\text{tr}(\bar{\mathbf{P}}_k^T \mathbf{C}_{\text{r}_p}^{-1} \bar{\mathbf{P}}_k^*) \text{tr}(\bar{\mathbf{P}}_{k'}^T \mathbf{C}_{\text{r}_p}^{-1} \bar{\mathbf{P}}_{k'}^*)}} \quad (65)$$

$$= \frac{\mathbf{p}_k^T \Phi^{-1} \mathbf{p}_{k'}^*}{\sqrt{(\mathbf{p}_k^T \Phi^{-1} \mathbf{p}_k^*)(\mathbf{p}_{k'}^T \Phi^{-1} \mathbf{p}_{k'}^*)}} \quad (66)$$

where (66) is equal to zero if  $\mathbf{P}$  is chosen such that  $\mathbf{P}\mathbf{P}^H$  is circulant (as in the case of DFT pilot matrix), which

implies that  $\mathbf{p}_k^T \Phi^{-1} \mathbf{p}_{k'}^* = 0$  [17]. However, for a given  $\rho$ , we cannot make  $\mathbb{E}[\hat{\mathbf{h}}_k^H \hat{\mathbf{h}}_{k'}] \rightarrow 0$  and therefore the asymptotic orthogonality does not hold in general. Nevertheless, it can be shown that  $\mathbb{E}[\hat{\mathbf{h}}_k^H \hat{\mathbf{h}}_{k'}] \rightarrow 0$  as  $\tau \rightarrow \infty$  and  $\rho \rightarrow 0$ . This is because the channel estimation error can be made arbitrarily small by simultaneously increasing  $\tau$  and decreasing  $\rho$  [17].

### APPENDIX III DERIVATIONS OF THE LMMD RECEIVER

Consider the reformulated receiver design problem in (30), obtained by imposing the MRC receiver in the inner expectation of (29). Then, we use the Bussgang decomposition to rewrite  $\mathbf{r}$  in (9) as

$$\mathbf{r} = \mathbf{G}(\mathbf{x})\mathbf{y} + \mathbf{d} \quad (67)$$

where  $\mathbf{d} \in \mathbb{C}^M$  is the quantization distortion vector that is uncorrelated with  $\mathbf{y}$  and  $\mathbf{G}(\mathbf{x})$  is defined in (33). Note that, for given  $\mathbf{H}$  and  $\mathbf{x}$ , we have  $\mathbf{y} \sim \mathcal{CN}(\sqrt{\rho}\mathbf{H}\mathbf{x}, \mathbf{I}_M)$ , which yields  $\mathbf{C}_{\mathbf{y}|\mathbf{x}} = \rho\mathbf{H}\mathbf{x}\mathbf{x}^H\mathbf{H}^H + \mathbf{I}_M$ . Furthermore, let  $\zeta_m \triangleq \sqrt{\rho}\mathbf{g}_m^T\mathbf{x}$ , where  $\mathbf{g}_m \in \mathbb{C}^M$  denotes the  $m$ th column of  $\mathbf{H}^T$ . Then, the  $(n, m)$ th element of  $\mathbf{C}_{\mathbf{y}|\mathbf{x}}$  can be written as in (68)–(69) at the end of the document, where the term  $\mathbb{E}[\text{Re}[y_n] \text{sgn}(\text{Re}[y_m])]$  is given in (70) at the end of the document. The remaining terms have a similar form and are thus omitted. Following similar steps, we derive  $\mathbf{C}_{\mathbf{r}|\mathbf{x}} \triangleq \mathbb{E}_{\mathbf{z}}[\mathbf{r}\mathbf{r}^H|\mathbf{x}] \in \mathbb{C}^{M \times M}$  as in (71) at the end of the document. Then,  $\mathbf{C}_{\mathbf{r}}$  defined in Section IV is given by

$$\mathbf{C}_{\mathbf{r}} = \mathbb{E}_{\mathbf{x}}[\mathbf{C}_{\mathbf{r}|\mathbf{x}}] = \frac{1}{L^K} \sum_{\mathbf{x} \in \mathcal{S}^K} \mathbf{C}_{\mathbf{r}|\mathbf{x}}. \quad (72)$$

Now, the LMMD receiver can be obtained by setting the derivative of the objective of (30) to zero, which yields

$$\mathbf{V}^{(\text{LMMD})} = \mathbf{C}_{\mathbf{r}}^{-1} \mathbb{E}_{\mathbf{x}, \mathbf{z}}[\mathbf{r}\mathbf{e}(\mathbf{x})^H] \quad (73)$$

with  $\mathbf{e}(\mathbf{x})$  defined in (32). Since  $\mathbf{C}_{\mathbf{r}}$  can be rank deficient at high SNR, as  $\Phi(\cdot)$  in (71) quickly saturates to 1 or  $-1$ , we replace  $\mathbf{C}_{\mathbf{r}}^{-1}$  by its pseudo-inverse and obtain (31).

### APPENDIX IV FORMULATION OF RML

Let  $\tilde{\mathbf{x}} \triangleq [\text{Re}[\mathbf{x}], \text{Im}[\mathbf{x}]]^T \in \mathbb{C}^{2K}$ ,  $\tilde{\mathbf{r}} \triangleq [\text{Re}[\mathbf{r}], \text{Im}[\mathbf{r}]]^T \in \mathbb{C}^{2M}$ , and

$$\tilde{\mathbf{G}} \triangleq \begin{bmatrix} \text{Re}[\mathbf{H}] & -\text{Im}[\mathbf{H}] \\ \text{Im}[\mathbf{H}] & \text{Re}[\mathbf{H}] \end{bmatrix}^T \in \mathbb{C}^{2K \times 2M}. \quad (74)$$

RML obtains the data symbol vector  $\mathbf{x}^*$  that minimizes the RML function, i.e., [14]

$$\mathbf{x}^* = \underset{\mathbf{x} \in \mathcal{S}^K}{\text{argmin}} \sum_{m=1}^{2M} \log(1 + e^{-\theta \tilde{r}_m \tilde{\mathbf{g}}_m^T \tilde{\mathbf{x}}}) \quad (75)$$

where  $\tilde{r}_m$  is the  $m$ th element of  $\tilde{\mathbf{r}}$ ,  $\tilde{\mathbf{g}}_m \in \mathbb{C}^{2K}$  is the  $m$ th column of  $\tilde{\mathbf{G}}$ , and  $\theta = 1.702 \times \sqrt{\frac{4\rho}{\rho K + 1}}$ .

### REFERENCES

[1] A. Radbord, I. Atzeni, and A. Tölli, “Multi-user data detection in massive MIMO with 1-bit ADCs,” in *Proc. IEEE Int. Conf. Acoust., Speech, and Signal Process. (ICASSP)*, 2023.

[2] A. Radbord, I. Atzeni, and A. Tölli, “Enhanced data detection for massive MIMO with 1-bit ADCs,” in *Proc. Asilomar Conf. Signals, Syst., and Comput. (ASILOMAR)*, 2023.

[3] N. Rajatheva, I. Atzeni, E. Björnson *et al.*, “White paper on broadband connectivity in 6G,” <https://oulurepo oulu.fi/handle/10024/36613>, 2020.

[4] I. Atzeni, A. Tölli, D. H. N. Nguyen, and A. L. Swindlehurst, “Doubly 1-bit quantized massive MIMO,” in *Proc. Asilomar Conf. Signals, Syst., and Comput. (ASILOMAR)*, 2023.

[5] Y. Li, C. Tao, G. Seco-Granados, A. Mezghani, A. L. Swindlehurst, and L. Liu, “Channel estimation and performance analysis of one-bit massive MIMO systems,” *IEEE Trans. Signal Process.*, vol. 65, no. 15, pp. 4075–4089, 2017.

[6] S. Jacobsson, G. Durisi, M. Coldrey, U. Gustavsson, and C. Studer, “Throughput analysis of massive MIMO uplink with low-resolution ADCs,” *IEEE Trans. Wireless Commun.*, vol. 16, no. 6, pp. 1304–1309, 2017.

[7] I. Atzeni, A. Tölli, and G. Durisi, “Low-resolution massive MIMO under hardware power consumption constraints,” in *Proc. Asilomar Conf. Signals, Syst., and Comput. (ASILOMAR)*, 2021.

[8] K. Roth, H. Pirzadeh, A. L. Swindlehurst, and J. Nossek, “A comparison of hybrid beamforming and digital beamforming with low-resolution ADCs for multiple users and imperfect CSI,” *IEEE J. Sel. Topics Signal Process.*, vol. 12, no. 3, pp. 484–498, 2018.

[9] A. Saxena, I. Fijalkow, and A. L. Swindlehurst, “Analysis of one-bit quantized precoding for the multiuser massive MIMO downlink,” *IEEE Trans. Signal Process.*, vol. 65, no. 17, pp. 4624–4634, 2017.

[10] J. Choi, J. Mo, and R. W. Heath, “Near maximum-likelihood detector and channel estimator for uplink multiuser massive MIMO systems with one-bit ADCs,” *IEEE Trans. Wireless Commun.*, vol. 64, no. 5, pp. 2005–2018, 2016.

[11] S. Wang, Y. Li, and J. Wang, “Multiuser detection in massive spatial modulation MIMO with low-resolution ADCs,” *IEEE Trans. Wireless Commun.*, vol. 14, no. 4, pp. 2156–2168, 2015.

[12] Y.-S. Jeon, N. Lee, S.-N. Hong, and R. W. Heath, “One-bit sphere decoding for uplink massive MIMO systems with one-bit ADCs,” *IEEE Trans. Wireless Commun.*, vol. 17, no. 7, pp. 4509–4521, 2018.

[13] I. Watanabe, T. Takahashi, S. Ibi, A. Tölli, and S. Sampei, “Gaussian belief propagation for mmWave large MIMO detection with low-resolution ADCs,” in *Proc. IEEE Int. Workshop Signal Process. Adv. in Wireless Commun. (SPAWC)*, 2022.

[14] L. V. Nguyen, A. L. Swindlehurst, and D. H. N. Nguyen, “Linear and deep neural network-based receivers for massive MIMO systems with one-bit ADCs,” *IEEE Trans. Wireless Commun.*, vol. 20, no. 11, pp. 7333–7345, 2021.

[15] K. Gao, N. J. Estes, B. Hochwald, J. Chisum, and J. N. Laneman, “Power-performance analysis of a simple one-bit transceiver,” in *Proc. Inf. Theory and Appl. Workshop (ITA)*, 2017.

[16] L. V. Nguyen, A. L. Swindlehurst, and D. H. N. Nguyen, “SVM-based channel estimation and data detection for one-bit massive MIMO systems,” *IEEE Trans. Signal Process.*, vol. 69, pp. 2086–2099, 2021.

[17] I. Atzeni and A. Tölli, “Channel estimation and data detection analysis of massive MIMO with 1-bit ADCs,” *IEEE Trans. Wireless Commun.*, vol. 21, no. 6, pp. 3850–3867, 2022.

[18] I. Atzeni and A. Tölli, “Uplink data detection analysis of 1-bit quantized massive MIMO,” in *Proc. IEEE Int. Workshop Signal Process. Adv. in Wireless Commun. (SPAWC)*, 2021.

[19] D. Abdelhameed, K. Umehayashi, I. Atzeni, and A. Tölli, “Enhanced signal detection and constellation design for massive SIMO communications with 1-bit ADCs,” *IEEE Access*, vol. 11, pp. 11 749–11 765, 2023.

[20] E. Björnson, J. Hoydis, and L. Sanguinetti, “Massive MIMO networks: Spectral, energy, and hardware efficiency,” *Found. and Trends Signal Process.*, vol. 11, no. 3–4, pp. 154–655, 2017.

[21] H. Yin, D. Gesbert, M. Filippou, and Y. Liu, “A coordinated approach to channel estimation in large-scale multiple-antenna systems,” *IEEE J. Sel. Areas Commun.*, vol. 31, no. 2, pp. 264–273, 2013.

[22] M. Hyder and K. Mahata, “Zadoff-Chu sequence design for random access initial uplink synchronization in LTE-like systems,” *IEEE Trans. Wireless Commun.*, vol. 16, no. 1, pp. 503–511, 2017.

[23] R. Couillet and M. Debbah, *Random Matrix Methods for Wireless Communications*. Cambridge University Press, 2011.

$$\mathbb{E}[r_m r_{p,n,u}^*] = (\rho K + 1) \left[ \Omega \left( \frac{\rho \sum_{k=1}^K \sum_{i=1}^M \operatorname{Re} [[\mathbf{C}_{\mathbf{h}_k}^{\frac{1}{2}}]_{m,i} [\mathbf{C}_{\mathbf{h}_k}^{\frac{1}{2}}]_{n,i}^* x_k P_{u,k}]}{(\rho \sum_{k=1}^K \sum_{i=1}^M |[\mathbf{C}_{\mathbf{h}_k}^{\frac{1}{2}}]_{m,i} x_k|^2 + 1)^{\frac{1}{2}} (\rho \sum_{k=1}^K \sum_{i=1}^M |[\mathbf{C}_{\mathbf{h}_k}^{\frac{1}{2}}]_{n,i}|^2 + 1)^{\frac{1}{2}}} \right) + j \Omega \left( \frac{\rho \sum_{k=1}^K \sum_{i=1}^M \operatorname{Im} [[\mathbf{C}_{\mathbf{h}_k}^{\frac{1}{2}}]_{m,i} [\mathbf{C}_{\mathbf{h}_k}^{\frac{1}{2}}]_{n,i}^* x_k P_{u,k}]}{(\rho \sum_{k=1}^K \sum_{i=1}^M |[\mathbf{C}_{\mathbf{h}_k}^{\frac{1}{2}}]_{m,i} x_k|^2 + 1)^{\frac{1}{2}} (\rho \sum_{k=1}^K \sum_{i=1}^M |[\mathbf{C}_{\mathbf{h}_k}^{\frac{1}{2}}]_{n,i}|^2 + 1)^{\frac{1}{2}}} \right) \right] \quad (49)$$

$$\mathbb{E}[a_m A_{n,u}] = \Omega \left( \frac{\rho \sum_{k=1}^K \sum_{i=1}^M \operatorname{Re} [[\mathbf{C}_{\mathbf{h}_k}^{\frac{1}{2}}]_{m,i} [\mathbf{C}_{\mathbf{h}_k}^{\frac{1}{2}}]_{n,i}^* x_k P_{u,k}]}{(\rho \sum_{k=1}^K \sum_{i=1}^M |[\mathbf{C}_{\mathbf{h}_k}^{\frac{1}{2}}]_{m,i} x_k|^2 + 1)^{\frac{1}{2}} (\rho \sum_{k=1}^K \sum_{i=1}^M |[\mathbf{C}_{\mathbf{h}_k}^{\frac{1}{2}}]_{n,i}|^2 + 1)^{\frac{1}{2}}} \right) \quad (50)$$

$$\zeta = [\operatorname{Re}[\bar{h}_{1,1}], \dots, \operatorname{Re}[\bar{h}_{M,1}], \dots, \operatorname{Re}[\bar{h}_{1,K}], \dots, \operatorname{Re}[\bar{h}_{M,K}], \operatorname{Im}[\bar{h}_{1,1}], \dots, \operatorname{Im}[\bar{h}_{M,1}], \dots, \operatorname{Im}[\bar{h}_{1,K}], \dots, \operatorname{Im}[\bar{h}_{M,K}], \operatorname{Re}[z_{p,n,u}], \operatorname{Re}[z_m]]^T \sim \mathcal{N} \left( \mathbf{0}_{(2MK+2)}, \frac{1}{2} \mathbf{I}_{(2MK+2)} \right), \quad (51)$$

$$\mathbf{a}_1^{(m)} = \sqrt{\rho} \left[ \operatorname{Re} [[\mathbf{C}_{\mathbf{h}_1}^{\frac{1}{2}}]_{m,1} x_1], \dots, \operatorname{Re} [[\mathbf{C}_{\mathbf{h}_1}^{\frac{1}{2}}]_{m,M} x_1], \dots, \operatorname{Re} [[\mathbf{C}_{\mathbf{h}_K}^{\frac{1}{2}}]_{m,1} x_K], \dots, \operatorname{Re} [[\mathbf{C}_{\mathbf{h}_K}^{\frac{1}{2}}]_{m,M} x_K], \right. \\ \left. - \operatorname{Im} [[\mathbf{C}_{\mathbf{h}_1}^{\frac{1}{2}}]_{m,1} x_1], \dots, -\operatorname{Im} [[\mathbf{C}_{\mathbf{h}_1}^{\frac{1}{2}}]_{m,M} x_1], \dots, -\operatorname{Im} [[\mathbf{C}_{\mathbf{h}_K}^{\frac{1}{2}}]_{m,1} x_K], \dots, -\operatorname{Im} [[\mathbf{C}_{\mathbf{h}_K}^{\frac{1}{2}}]_{m,M} x_K], 0, 1 \right]^T \\ \in \mathbb{R}^{(2MK+2)}, \quad (52)$$

$$\mathbf{a}_2^{(n,u)} = \sqrt{\rho} \left[ \operatorname{Re} [[\mathbf{C}_{\mathbf{h}_1}^{\frac{1}{2}}]_{n,1} P_{u,1}^*], \dots, \operatorname{Re} [[\mathbf{C}_{\mathbf{h}_1}^{\frac{1}{2}}]_{n,M} P_{u,1}^*], \dots, \operatorname{Re} [[\mathbf{C}_{\mathbf{h}_K}^{\frac{1}{2}}]_{n,1} P_{u,K}^*], \dots, \operatorname{Re} [[\mathbf{C}_{\mathbf{h}_K}^{\frac{1}{2}}]_{n,M} P_{u,K}^*], \right. \\ \left. - \operatorname{Im} [[\mathbf{C}_{\mathbf{h}_1}^{\frac{1}{2}}]_{n,1} P_{u,1}^*], \dots, -\operatorname{Im} [[\mathbf{C}_{\mathbf{h}_1}^{\frac{1}{2}}]_{n,M} P_{u,1}^*], \dots, -\operatorname{Im} [[\mathbf{C}_{\mathbf{h}_K}^{\frac{1}{2}}]_{n,1} P_{u,K}^*], \dots, -\operatorname{Im} [[\mathbf{C}_{\mathbf{h}_K}^{\frac{1}{2}}]_{n,M} P_{u,K}^*], 1, 0 \right]^T \\ \in \mathbb{R}^{(2MK+2)} \quad (53)$$

$$\mathbb{E} \left[ \operatorname{sgn} \left( \sqrt{\rho} \sum_{k=1}^K \sum_{i=1}^M (\operatorname{Re}[\bar{h}_{i,k}] \operatorname{Re} [[\mathbf{C}_{\mathbf{h}_k}^{\frac{1}{2}}]_{m,i} x_k] - \operatorname{Im}[\bar{h}_{i,k}] \operatorname{Im} [[\mathbf{C}_{\mathbf{h}_k}^{\frac{1}{2}}]_{m,i} x_k]) + \operatorname{Re}[z_m] \right) \right. \\ \left. \times \operatorname{sgn} \left( \sqrt{\rho} \sum_{k=1}^K \sum_{i=1}^M (\operatorname{Re}[\bar{h}_{i,k}] \operatorname{Re} [[\mathbf{C}_{\mathbf{h}_k}^{\frac{1}{2}}]_{n,i} P_{u,k}^*] - \operatorname{Im}[\bar{h}_{i,k}] \operatorname{Im} [[\mathbf{C}_{\mathbf{h}_k}^{\frac{1}{2}}]_{n,i} P_{u,k}^*]) + \operatorname{Re}[z_{p,n,u}] \right) \right] \\ = \Omega \left( \frac{\rho \sum_{k=1}^K \sum_{i=1}^M (\operatorname{Re} [[\mathbf{C}_{\mathbf{h}_k}^{\frac{1}{2}}]_{m,i} x_k] \operatorname{Re} [[\mathbf{C}_{\mathbf{h}_k}^{\frac{1}{2}}]_{n,i} P_{u,k}^*] + \operatorname{Im} [[\mathbf{C}_{\mathbf{h}_k}^{\frac{1}{2}}]_{m,i} x_k] \operatorname{Im} [[\mathbf{C}_{\mathbf{h}_k}^{\frac{1}{2}}]_{n,i} P_{u,k}^*])}{\left( \rho \sum_{k=1}^K \sum_{i=1}^M (\operatorname{Re} [[\mathbf{C}_{\mathbf{h}_k}^{\frac{1}{2}}]_{m,i} x_k]^2 + \operatorname{Im} [[\mathbf{C}_{\mathbf{h}_k}^{\frac{1}{2}}]_{m,i} x_k]^2) + 1 \right)^{\frac{1}{2}} \left( \rho \sum_{k=1}^K \sum_{i=1}^M (\operatorname{Re} [[\mathbf{C}_{\mathbf{h}_k}^{\frac{1}{2}}]_{n,i} P_{u,k}^*]^2 + \operatorname{Im} [[\mathbf{C}_{\mathbf{h}_k}^{\frac{1}{2}}]_{n,i} P_{u,k}^*]^2) + 1 \right)^{\frac{1}{2}}} \right) \quad (54)$$

$$\hat{\mathbf{h}}_k^H \hat{\mathbf{h}}_{k'} = \rho \mathbf{r}_p^H \mathbf{X}_k^H \mathbf{X}_{k'} \mathbf{r}_p = \rho^2 \bar{\mathbf{h}}^H \mathbf{C}_{\mathbf{h}}^{\frac{1}{2}} \bar{\mathbf{P}}^T \mathbf{A}_p \mathbf{X}_k^H \mathbf{X}_{k'} \mathbf{A}_p \bar{\mathbf{P}}^* \mathbf{C}_{\mathbf{h}}^{\frac{1}{2}} \bar{\mathbf{h}} + \rho^{\frac{3}{2}} \bar{\mathbf{h}}^H \mathbf{C}_{\mathbf{h}}^{\frac{1}{2}} \bar{\mathbf{P}}^T \mathbf{A}_p \mathbf{X}_k^H \mathbf{X}_{k'} \mathbf{C}_{\mathbf{n}}^{\frac{1}{2}} \bar{\mathbf{n}} \\ + \rho^{\frac{3}{2}} \bar{\mathbf{n}}^H \mathbf{C}_{\mathbf{n}}^{\frac{1}{2}} \mathbf{X}_k^H \mathbf{X}_{k'} \mathbf{A}_p \bar{\mathbf{P}}^* \mathbf{C}_{\mathbf{h}}^{\frac{1}{2}} \bar{\mathbf{h}} + \bar{\mathbf{n}}^H \mathbf{C}_{\mathbf{n}}^{\frac{1}{2}} \mathbf{X}_k^H \mathbf{X}_{k'} \mathbf{C}_{\mathbf{n}}^{\frac{1}{2}} \bar{\mathbf{n}} \quad (58)$$

$$\frac{\hat{\mathbf{h}}_k^H \hat{\mathbf{h}}_{k'}}{\sqrt{\mathbb{E}[\|\hat{\mathbf{h}}_k\|^2] \mathbb{E}[\|\hat{\mathbf{h}}_{k'}\|^2]}} \rightarrow \frac{\rho^2 \operatorname{tr}(\mathbf{C}_{\mathbf{h}}^{\frac{1}{2}} \bar{\mathbf{P}}^T \mathbf{A}_p \mathbf{X}_k^H \mathbf{X}_{k'} \mathbf{A}_p \bar{\mathbf{P}}^* \mathbf{C}_{\mathbf{h}}^{\frac{1}{2}})}{\sqrt{\mathbb{E}[\|\hat{\mathbf{h}}_k\|^2] \mathbb{E}[\|\hat{\mathbf{h}}_{k'}\|^2]}} + \frac{\rho \operatorname{tr}(\mathbf{C}_{\mathbf{n}}^{\frac{1}{2}} \mathbf{X}_k^H \mathbf{X}_{k'} \mathbf{C}_{\mathbf{n}}^{\frac{1}{2}})}{\sqrt{\mathbb{E}[\|\hat{\mathbf{h}}_k\|^2] \mathbb{E}[\|\hat{\mathbf{h}}_{k'}\|^2]}} = \frac{\mathbb{E}[\hat{\mathbf{h}}_k^H \hat{\mathbf{h}}_{k'}]}{\sqrt{\mathbb{E}[\|\hat{\mathbf{h}}_k\|^2] \mathbb{E}[\|\hat{\mathbf{h}}_{k'}\|^2]}} \quad (63)$$

$$[\mathbf{C}_{\mathbf{y}|\mathbf{x}}]_{n,m} = \sqrt{\frac{\rho K + 1}{2}} \left( \mathbb{E}[\operatorname{Re}[y_n] \operatorname{sgn}(\operatorname{Re}[y_m])] + \mathbb{E}[\operatorname{Im}[y_n] \operatorname{sgn}(\operatorname{Im}[y_m])] \right. \\ \left. - j \mathbb{E}[\operatorname{Re}[y_n] \operatorname{sgn}(\operatorname{Im}[y_m])] + j \mathbb{E}[\operatorname{Im}[y_n] \operatorname{sgn}(\operatorname{Re}[y_m])] \right) \quad (68)$$

$$= \begin{cases} \sqrt{\frac{\rho K + 1}{2}} \left( \sqrt{\frac{1}{\pi}} (\exp(-\operatorname{Re}[\zeta_m]^2) + \exp(-\operatorname{Im}[\zeta_m]^2)) + \operatorname{Re}[\zeta_n \Phi(\zeta_m)] + j \operatorname{Im}[\zeta_n \Phi(\zeta_m^*)] \right) & \text{if } m = n, \\ \sqrt{\frac{\rho K + 1}{2}} \left( \operatorname{Re}[\zeta_n \Phi(\zeta_m^*)] + j \operatorname{Im}[\zeta_n \Phi(\zeta_m^*)] \right) & \text{otherwise} \end{cases} \quad (69)$$

$$\mathbb{E}[\operatorname{Re}[y_n] \operatorname{sgn}(\operatorname{Re}[y_m])] = \begin{cases} \sqrt{\frac{1}{\pi}} \exp(-\operatorname{Re}[\zeta_m]^2) + \operatorname{Re}[\zeta_n] \Phi(\operatorname{Re}[\zeta_m]) & \text{if } m = n, \\ \operatorname{Re}[\zeta_n] \Phi(\operatorname{Re}[\zeta_m]) & \text{otherwise} \end{cases} \quad (70)$$

$$[\mathbf{C}_{\mathbf{r}|\mathbf{x}}]_{n,m} = \begin{cases} \rho K + 1 & \text{if } m = n, \\ \frac{\rho K + 1}{2} \left( \operatorname{Re}[\Phi(\zeta_n) \Phi(\zeta_m^*)] + j \operatorname{Im}[\Phi(\zeta_n) \Phi(\zeta_m^*)] \right) & \text{otherwise} \end{cases} \quad (71)$$